RESEARCH ARTICLE

Zn^{2+} is essential for Ca^{2+} oscillations in mouse eggs

Hiroki Akizawa[1], Emily M Lopes[1,2], Rafael A Fissore[1]*

[1]Department of Veterinary and Animal Sciences, University of Massachusetts Amherst, Amherst, United States; [2]Molecular and Cellular Biology Graduate Program, University of Massachusetts, Amherst, United States

Abstract Changes in the intracellular concentration of free calcium (Ca^{2+}) underpin egg activation and initiation of development in animals and plants. In mammals, the Ca^{2+} release is periodical, known as Ca^{2+} oscillations, and mediated by the type 1 inositol 1,4,5-trisphosphate receptor (IP_3R1). Another divalent cation, zinc (Zn^{2+}), increases exponentially during oocyte maturation and is vital for meiotic transitions, arrests, and polyspermy prevention. It is unknown if these pivotal cations interplay during fertilization. Here, using mouse eggs, we showed that basal concentrations of labile Zn^{2+} are indispensable for sperm-initiated Ca^{2+} oscillations because Zn^{2+}-deficient conditions induced by cell-permeable chelators abrogated Ca^{2+} responses evoked by fertilization and other physiological and pharmacological agonists. We also found that chemically or genetically generated eggs with lower levels of labile Zn^{2+} displayed reduced IP_3R1 sensitivity and diminished ER Ca^{2+} leak despite the stable content of the stores and IP_3R1 mass. Resupplying Zn^{2+} restarted Ca^{2+} oscillations, but excessive Zn^{2+} prevented and terminated them, hindering IP_3R1 responsiveness. The findings suggest that a window of Zn^{2+} concentrations is required for Ca^{2+} responses and IP_3R1 function in eggs, ensuring optimal response to fertilization and egg activation.

***For correspondence:** rfissore@umass.edu

Competing interest: The authors declare that no competing interests exist.

Funding: See page 18

Sent for Review
13 April 2023
Preprint posted
17 April 2023
Reviewed preprint posted
27 June 2023
Reviewed preprint revised
20 November 2023
Version of Record published
15 December 2023

Reviewing Editor: Darryl L Russell, University of Adelaide, Australia

eLife assessment

This article reports an **important** series of results showing the relationship between oscillatory zinc and calcium fluctuations during egg activation and fertilization. **Compelling** evidence using several complimentary approaches provides further insight into the signals for proper egg activation that underpin successful fertilization and embryo development. The findings are significant because they may lead to improvements in assisted reproduction methods.

Introduction

Vertebrate eggs are arrested at the metaphase stage of the second meiosis (MII) when ovulated because they have an active Cdk1/cyclin B complex and inactive APC/C^{Cdc20} (***Heim et al., 2018***). Release from MII initiates egg activation, the first hallmark of embryonic development (***Ducibella et al., 2002***; ***Schultz and Kopf, 1995***). The universal signal of egg activation is an increase in the intracellular concentration of calcium (Ca^{2+}) (***Ridgway et al., 1977***; ***Stricker, 1999***). Ca^{2+} release causes the inactivation of the APC/C inhibitor Emi2, which enhances cyclin B degradation and induces meiotic exit (***Lorca et al., 1993***; ***Shoji et al., 2006***; ***Suzuki et al., 2010a***). In mammals, the stereotypical fertilization Ca^{2+} signal, oscillations, consists of transient but periodical Ca^{2+} increases that promote progression into interphase (***Deguchi et al., 2000***; ***Miyazaki et al., 1986***). The sperm-borne phospholipase C zeta1 (PLC ζ) persistently stimulates the production of inositol 1,4,5-trisphosphate (IP_3) (***Matsu-ura et al., 2019***; ***Saunders et al., 2002***; ***Wu et al., 2001***) that binds its cognate receptor in the endoplasmic reticulum (ER), IP_3R1, and causes Ca^{2+} release from the egg's main Ca^{2+} reservoir

(**Wakai et al., 2019**). The intake of extracellular Ca^{2+} via plasma membrane channels and transporters ensures the persistence of the oscillations (**Miao et al., 2012**; **Stein et al., 2020**; **Wakai et al., 2019**; **Wakai et al., 2013**).

Before fertilization, maturing oocytes undergo cellular and biochemical modifications (see for review **Ajduk et al., 2008**). The nucleus of immature oocytes, known as the germinal vesicle (GV), undergoes the breakdown of its envelope, marking the onset of maturation and setting in motion a series of cellular events that culminate with the release of the first polar body, the correct ploidy for fertilization, and re-arrest at MII (**Eppig, 1996**). Other organelles are also reorganized, such as cortical granules migrate to the cortex for exocytosis and polyspermy block, mitochondria undergo repositioning, and the cytoplasm's redox state becomes progressively reduced to promote the exchange of the sperm's protamine load (**Liu, 2011**; **Perreault et al., 1988**; **Wakai et al., 2014**). Wide-ranging adaptations also occur in the Ca^{2+} release machinery to produce timely and protracted Ca^{2+} oscillations following sperm entry (**Fujiwara et al., 1993**; **Lawrence et al., 1998**), including the increase in the content of the Ca^{2+} stores, ER reorganization with cortical cluster formation, and increased IP_3R1 sensitivity (**Lee et al., 2006**; **Wakai et al., 2012**). The total intracellular levels of zinc (Zn^{2+}) also remarkably increase during maturation, amounting to a 50% rise, which is necessary for oocytes to proceed to the telophase I of meiosis and beyond (**Kim et al., 2010**). Notably, after fertilization, Zn^{2+} levels need to decrease, as Emi2 is a Zn^{2+}-associated molecule, and high Zn^2 levels prevent MII exit (**Bernhardt et al., 2012**; **Shoji et al., 2014**; **Suzuki et al., 2010b**). Following the initiation of Ca^{2+} oscillations, approximately 10–20% of the Zn^{2+} accrued during maturation is ejected during the Zn^{2+} sparks, a conserved event in vertebrates and invertebrate species (**Converse and Thomas, 2020**; **Kim et al., 2011**; **Mendoza et al., 2022**; **Que et al., 2019**; **Seeler et al., 2021**; **Tokuhiro and Dean, 2018**; **Wozniak et al., 2020**; **Zhang et al., 2016**). The use of Zn^{2+} chelators such as N,N,N,N-tetrakis (2-pyridinylmethyl)–1,2-ethylenediam ine (TPEN) to create Zn^{2+}-deficient conditions buttressed the importance of Zn^{2+} during meiotic transitions (**Kim et al., 2010**; **Suzuki et al., 2010b**). However, whether the analogous dynamics of Ca^{2+} and Zn^{2+} during maturation imply crosstalk and Zn^{2+} levels modulate Ca^{2+} release during fertilization is unknown.

IP_3Rs are the most abundant intracellular Ca^{2+} release channel in non-muscle cells (**Berridge, 2016**). They form a channel by assembling into tetramers with each subunit of ~270 kDa MW (**Taylor and Tovey, 2010**). Mammalian eggs express the type I IP_3R, the most widespread isoform (**Fissore et al., 1999**; **Parrington et al., 1998**). IP_3R1 is essential for egg activation because its inhibition precludes Ca^{2+} oscillations (**Miyazaki and Ito, 2006**; **Miyazaki et al., 1992**; **Xu et al., 2003**). Myriad and occasionally cell-specific factors influence Ca^{2+} release through the IP_3R1 (**Taylor and Tovey, 2010**). For example, following fertilization, IP_3R1 undergoes ligand-induced degradation caused by the sperm-initiated long-lasting production of IP_3 that effectively reduces the IP_3R1 mass (**Brind et al., 2000**; **Jellerette et al., 2000**). Another regulatory mechanism is Ca^{2+}, a universal cofactor, which biphasically regulates IP_3Rs' channel opening (**Iino, 1990**; **Jean and Klee, 1986**), congruent with several Ca^{2+} and calmodulin binding sites on the channel's sequence (**Sienaert et al., 1997**; **Sipma et al., 1999**). Notably, Zn^{2+} may also participate in IP_3R1 regulation. Recent studies using electron cryomicroscopy (cryoEM), a technique that allows peering into the structure of IP_3R1 with a near-atomic resolution, have revealed that a helical linker (LNK) domain near the C-terminus mediates the coupling between the N- and C-terminal ends necessary for channel opening (**Fan et al., 2015**). The LNK domain contains a putative zinc-finger motif proposed to be vital for IP_3R1 function (**Fan et al., 2015**; **Paknejad and Hite, 2018**). Therefore, the exponential increase in Zn^{2+} levels in maturing oocytes, besides its essential role in meiosis progression, may optimize the IP_3R1 function, revealing hitherto unknown cooperation between these cations during fertilization.

Here, we examined whether crosstalk between Ca^{2+} and Zn^{2+} is required to initiate and sustain Ca^{2+} oscillations and maintain Ca^{2+} store content in MII eggs. We found that Zn^{2+}-deficient conditions inhibited Ca^{2+} release and oscillations without reducing Ca^{2+} stores, IP_3 production, IP_3R1 expression, or altering the viability of eggs or zygotes. We show instead that Zn^{2+} deficiency impaired IP_3R1 function and lessened the receptor's ability to gate Ca^{2+} release out of the ER. Remarkably, resupplying Zn^{2+} re-established the oscillations interrupted by low Zn^{2+}, although persistent increases in intracellular Zn^{2+} were harmful, disrupting the Ca^{2+} responses and preventing egg activation. Together, the results show that besides contributing to oocyte maturation, Zn^{2+} has a central function in Ca^{2+} homeostasis

such that optimal Zn^{2+} concentrations ensure IP_3R1 function and the Ca^{2+} oscillations required for initiating embryo development.

Results

TPEN dose-dependently lowers intracellular Zn^{2+} and inhibits sperm-initiated Ca^{2+} oscillations

TPEN is a cell-permeable, non-specific chelator with a high affinity for transition metals widely used to study their function in cell physiology (***Arslan et al., 1985***; ***Lo et al., 2020***). Mouse oocytes and eggs have exceedingly high intracellular concentrations of Zn^{2+} (***Kim et al., 2011***; ***Kim et al., 2010***), and the TPEN-induced defects in the progression of meiosis have been ascribed to its chelation (***Bernhardt et al., 2011***; ***Kim et al., 2010***). In support of this view, the Zn^{2+} levels of cells showed acute reduction after TPEN addition, as reported by indicators such as FluoZin-3 (***Arslan et al., 1985***; ***Gee et al., 2002***; ***Suzuki et al., 2010b***). Studies in mouse eggs also showed that the addition of low µM (40–100) concentrations of TPEN disrupted Ca^{2+} oscillations initiated by fertilization or $SrCl_2$ (***Lawrence et al., 1998***; ***Suzuki et al., 2010b***), but the mechanism(s) and target(s) of the inhibition remained unknown. To gain insight into this phenomenon, we first performed dose-titration studies to determine the effectiveness of TPEN in lowering Zn^{2+} in eggs. The addition of 2.5 µM TPEN protractedly reduced Zn^{2+} levels, whereas 5 and 10 µM TPEN acutely and persistently reduced FluoZin-3 fluorescence (***Figure 1A***). These concentrations of TPEN are higher than the reported free Zn^{2+} concentrations in cells, but within range of those found in typical culture conditions (***Lo et al., 2020***; ***Qin et al., 2011***). We next determined the concentrations of TPEN required to abrogate fertilization-initiated oscillations. Following intracytoplasmic sperm injection (ICSI), we monitored Ca^{2+} responses while increasing TPEN concentrations. As shown in ***Figure 1B***, 5 and 10 µM TPEN effectively blocked ICSI-induced Ca^{2+} oscillations in over half of the treated cells, and the remaining eggs, after a prolonged interval, resumed lower-frequency rises (***Figure 1B***, center panels). Finally, 50 µM or greater concentrations of TPEN permanently blocked these oscillations (***Figure 1B***, right panel). It is noteworthy that at the time of addition TPEN concentrations of 5 µM or above induce a sharp drop in basal Fura-2 F340/F380 ratios, consistent with Fura-2's high affinity for Zn^{2+} (***Snitsarev et al., 1996***).

We next used membrane-permeable and -impermeable chelators to assess whether TPEN inhibited Ca^{2+} oscillations by chelating Zn^{2+} from intracellular or extracellular compartments. The addition of the high-affinity but cell-impermeable Zn^{2+} chelators DTPA and EDTA neither terminated nor temporarily interrupted ICSI-induced Ca^{2+} oscillations (***Figure 1C***), although protractedly slowed them down, possibly because of chelation and lowering of external Ca^{2+} (***Figure 1C***). These results suggest that chelation of external Zn^{2+} does not affect the continuation of oscillations. We cannot determine that EDTA successfully chelated all external Zn^{2+}, but the evidence that the addition of EDTA to the monitoring media containing cell-impermeable FluoZin-3 caused a marked reduction in fluorescence suggests that a noticeable fraction of the available Zn^{2+} was sequestered (***Figure 1—figure supplement 1***). Similarly, injection of m*Plcz1* mRNA in eggs incubated in Ca^{2+} and Mg^{2+}-free media supplemented with EDTA, to maximize the chances of chelation of external Zn^{2+}, initiated low-frequency but persistent oscillations, and addition of Ca^{2+} and Mg^{2+} restored the physiological periodicity (***Figure 1—figure supplement 1***). Lastly, another Zn^{2+}-permeable chelator, TPA, blocked the ICSI-initiated Ca^{2+} oscillations but required higher concentrations than TPEN (***Figure 1D***). Collectively, the data suggest that basal levels of labile internal Zn^{2+} are essential to sustain the fertilization-initiated Ca^{2+} oscillations in eggs.

We next evaluated whether Zn^{2+} depletion prevented the completion of meiosis and pronuclear (PN) formation. To this end, ICSI-fertilized eggs were cultured in the presence of 10 µM TPEN for 8 hr, during which the events of egg activation were examined (***Figure 1E*** and ***Table 1***). All fertilized eggs promptly extruded second polar bodies regardless of treatment (***Figure 1E***). TPEN, however, impaired PN formation, and by 4 or 7 hr post-ICSI, most treated eggs failed to show PNs, unlike controls (***Figure 1E*** and ***Table 1***). Together, these results demonstrate that depletion of Zn^{2+} terminates Ca^{2+} oscillations and delays or prevents events of egg activation, including PN formation.

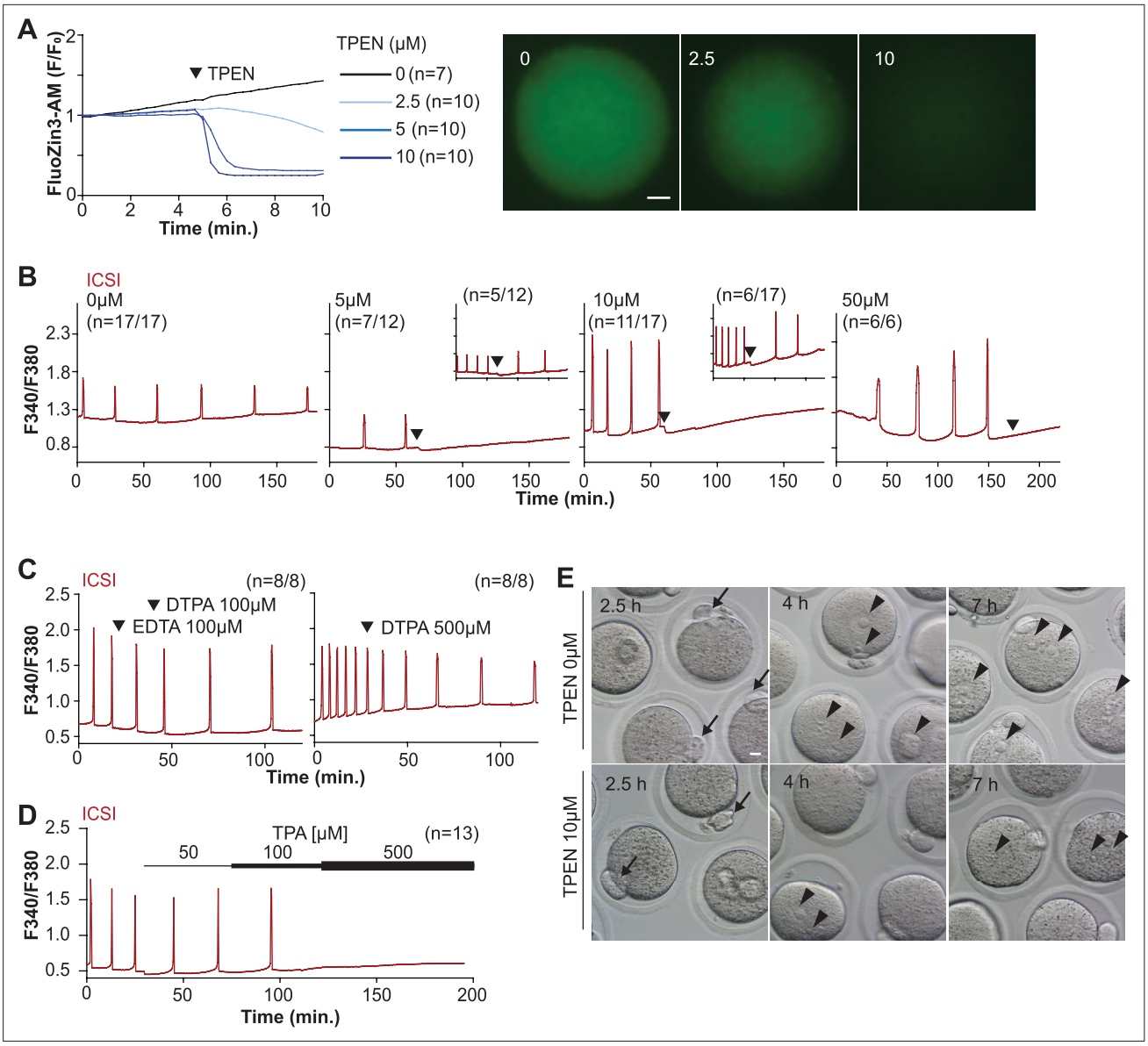

Figure 1. TPEN-induced Zn^{2+} deficiency inhibits fertilization-initiated Ca^{2+} oscillations in a dose-dependent manner. (**A**) Left panel: representative normalized Zn^{2+} recordings of MII eggs loaded with FluoZin-3AM following the addition of increasing concentrations of TPEN (0 μM, DMSO, black trace; 2.5 μM, sky blue; 5 μM, blue; 10 μM, navy). TPEN was directly added to the monitoring media. Right panel: representative fluorescent images of MII eggs loaded FluoZin-3AM supplemented with 0, 2.5, and 10 μM of TPEN. Scale bar: 10 μm. (**B–D**) (**B**) Representative Ca^{2+} oscillations following intracytoplasmic sperm injection (ICSI) after the addition of 0, 5, 10, or 50 μM TPEN (arrowheads). Insets show representative traces for eggs that resumed Ca^{2+} oscillations after TPEN. (**C**) As above, but following the addition of 100 μM EDTA, 100 or 500 μM DTPA (time of addition denoted by arrowheads). (**D**) Ca^{2+} oscillations following ICSI after the addition of 50, 100, and 500 μM TPA (horizontal bars of increasing thickness). (**E**) Representative bright field images of ICSI-fertilized eggs 2.5, 4, and 7 hr after sperm injection. Arrows and arrowheads denote the second polar body and pronuclear (PN) formation, respectively. Scale bar: 10 μm.

The online version of this article includes the following figure supplement(s) for figure 1:

Figure supplement 1. Cell-impermeable chelators effectively reduce Zn^{2+} levels in external media but do prevent initiation or continuation of Ca^{2+} oscillations.

TPEN is a universal inhibitor of Ca^{2+} oscillations in eggs

Mammalian eggs initiate Ca^{2+} oscillations in response to numerous stimuli and conditions (***Miyazaki and Ito, 2006***; ***Wakai and Fissore, 2013***). Fertilization and its release of PLC ζ stimulate the phosphoinositide pathway, producing IP_3 and Ca^{2+} oscillations (***Miyazaki, 1988***; ***Saunders et al., 2002***). Neurotransmitters such as acetylcholine (Ach) and other G-protein-coupled receptor agonists engage

Table 1. Addition of TPEN after intracytoplasmic sperm injection (ICSI) does not prevent extrusion of the second polar body but precludes pronuclear (PN) formation.

			PN	
Group*	**No. of zygotes**	**Second polar body (2.5 hr)**	**4 hr**	**7 hr**
Untreated	26	25 (96.1%)	23 (88.5%)	23 (88.5%)
TPEN (10 μM)	27	24 (88.9%)	1 (3.7%)***	2 (7.4%)***

***p<0.001.
*Data from three different replicates for each group.

a similar mechanism (***Dupont et al., 1996***; ***Kang et al., 2003***), although in these cases, IP_3 production occurs at the plasma membrane and is short-lived (***Kang et al., 2003***; ***Swann and Parrington, 1999***). Agonists such as $SrCl_2$ and thimerosal generate oscillations by sensitizing IP_3R1 without producing IP_3. The mechanism(s) of $SrCl_2$ is unclear, although its actions are reportedly directly on the IP_3R1 (***Hajnóczky and Thomas, 1997***; ***Hamada et al., 2003***; ***Nomikos et al., 2015***; ***Nomikos et al., 2011***; ***Sanders et al., 2018***). Thimerosal oxidizes dozens of thiol groups in the receptor, which enhances the receptor's sensitivity and ability to release Ca^{2+} (***Bootman et al., 1992***; ***Evellin et al., 2002***; ***Joseph et al., 2018***). We took advantage of the varied points at which the mentioned agonists engage the phosphoinositide pathway to examine TPEN's effectiveness in inhibiting their effects. m*Plcz1* mRNA injection, like fertilization, induces persistent Ca^{2+} oscillations, although m*Plcz1*'s tends to be more robust. Consistent with this, the addition of 10 and 25 μM TPEN transiently interrupted or belatedly terminated oscillations, whereas 50 μM acutely stopped all responses (***Figure 2A***). By contrast, $SrCl_2$-initiated rises were the most sensitive to Zn^{2+}-deficient conditions, with 2.5 μM TPEN nearly terminating all oscillations that 5 μM did (***Figure 2B***). TPEN was equally effective in ending the Ach-induced Ca^{2+} responses (***Figure 2C***), but curbing thimerosal responses required higher concentrations (***Figure 2D***). Lastly, we ruled out that downregulation of IP_3R1 was responsible for the slow-down or termination of the oscillations by TPEN. To accomplish this, we examined the IP_3R1 mass in eggs (***Jellerette et al., 2004***) with and without TPEN supplementation and injection of m*Plcz1* mRNA. By 4 hr post-injection, *Plcz1* induced the expected downregulation of IP_3R1 reactivity, whereas it was insignificant in TPEN-treated and *Plcz1* mRNA-injected eggs, as it was in uninjected control eggs (***Figure 2F***). These findings together show that Zn^{2+} deficiency inhibits the IP_3R1-mediated Ca^{2+} oscillations independently of IP_3 production or loss of receptor, suggesting a role of Zn^{2+} on IP_3R1 function (***Figure 2E***).

Zn^{2+} depletion reduces IP_3R1-mediated Ca^{2+} release

To directly assess the inhibitory effects of TPEN on IP_3R1 function, we used caged IP_3 (cIP_3) that, after short UV pulses, releases IP_3 into the ooplasm (***Wakai et al., 2012***; ***Walker et al., 1987***). To exclude the possible contribution of external Ca^{2+} to the responses, we performed the experiments in Ca^{2+}-free media. In response to sequential cIP_3 release 5 min apart, control eggs displayed corresponding Ca^{2+} rises that occasionally transitioned into short-lived oscillations (***Figure 3A***). The addition of TPEN after the third cIP_3 release prevented the subsequent Ca^{2+} response and prematurely terminated the in-progress Ca^{2+} rises (***Figure 3B***, inset). Pre-incubation of eggs with TPEN precluded cIP_3-induced Ca^{2+} release, even after 5 s UV exposure (***Figure 3C***). The addition of excess $ZnSO_4$ (100 μM) overcame TPEN's inhibitory effects only if added before (***Figure 3E***) and not after the addition of TPEN (***Figure 3D***). Similar concentrations of $MgCl_2$ or $CaCl_2$ failed to reverse TPEN effects (***Figure 3F and G***). Together, the results show that Zn^{2+} is required for IP_3R1-mediated Ca^{2+} release downstream of IP_3 production, appearing to interfere with receptor gating, as suggested by TPEN's rapid termination of in-progress Ca^{2+} rises and ongoing oscillations.

ERp44 is an ER luminal protein of the thioredoxin family that interacts with the IP_3R1, reportedly inhibiting its ability to mediate Ca^{2+} release (***Higo et al., 2005***). The localization of ERp44 in the ER-Golgi intermediate compartment of somatic cells correlates with Zn^{2+}'s availability and changes dramatically after TPEN treatment (***Higo et al., 2005***; ***Watanabe et al., 2019***). To rule out the possibility that TPEN suppresses the function of IP_3R1 by modifying the subcellular distribution of ERp44, we overexpressed ERp44 by injecting mRNA encoding HA-tagged ERp44 into MII eggs and monitored the effect on Ca^{2+} release. TPEN did not alter the localization of ERp44 (***Figure 3—figure***

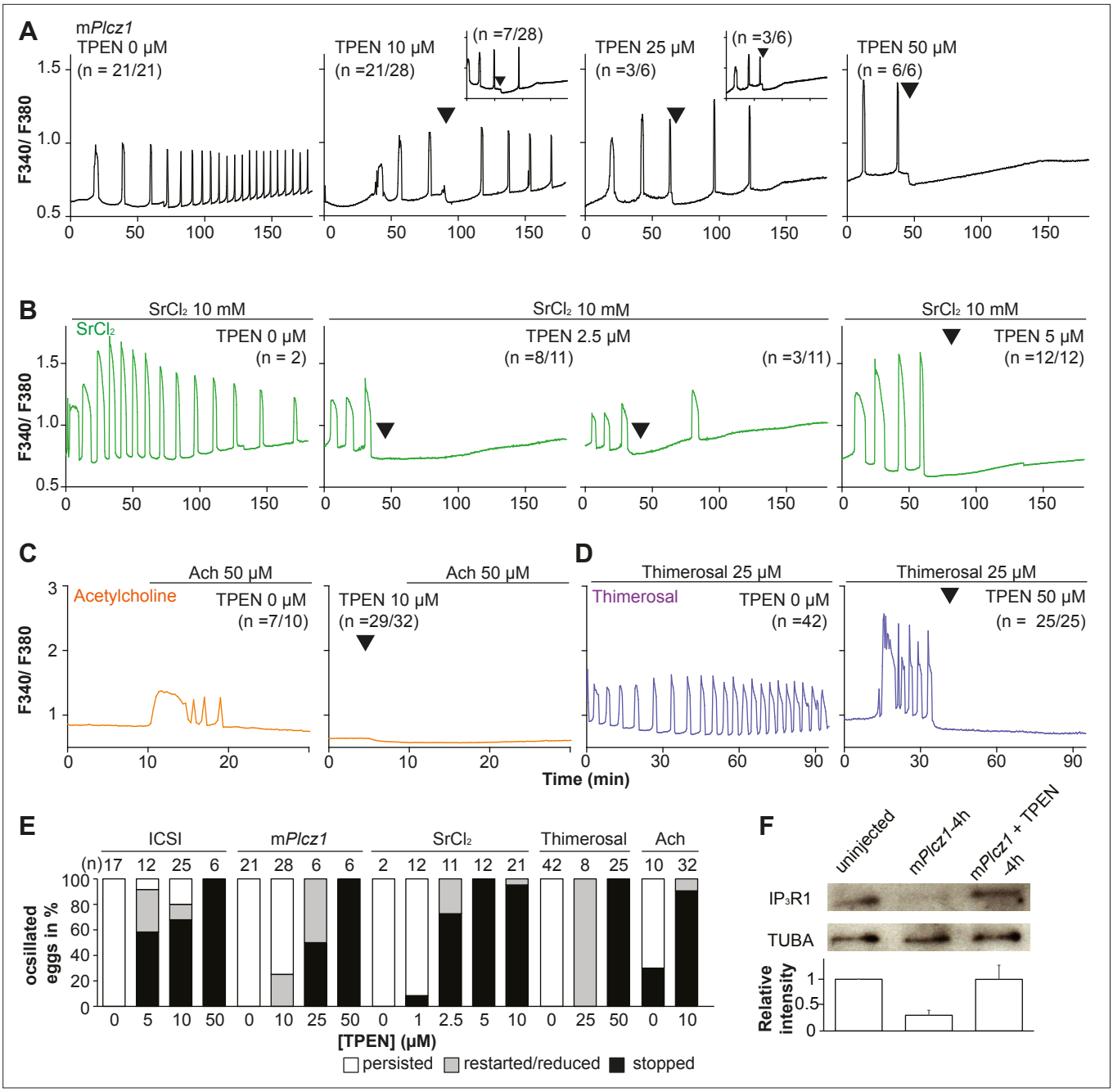

Figure 2. TPEN dose-dependently inhibits Ca^{2+} oscillations in eggs triggered by a broad spectrum of agonists that stimulate the PI pathway or IP_3R1. (**A–D**) Representative Ca^{2+} responses induced by (**A**) m*Plcz1* mRNA microinjection (0.01 μg/μl, black traces), (**B**) strontium chloride (10 mM, green), (**C**) acetylcholine chloride (50 μM, orange), and (**D**) thimerosal (25 μM, purple) in MII eggs. Increasing concentrations of TPEN were added to the monitoring media (arrowheads above traces denotes the time of adding). Insets in the upper row show representative traces of eggs that stop oscillating despite others continuing to oscillate. (**E**) Each bar graph summarizes the TPEN effect on Ca^{2+} oscillations at the selected concentrations for each of the agonists in (**A–D**). (**F**) Western blot showing the intensities of IP_3R1 and alpha-tubulin bands in MII eggs or in eggs injected with m*Plcz1* mRNA and incubated or not with TPEN above ($p<0.01$). Thirty eggs per lane in all cases. This experiment was repeated twice, and the mean relative intensity of each blot is shown in the bar graph below.

The online version of this article includes the following source data for figure 2:

Source data 1. IP_3R1 and TUBA western blottings.

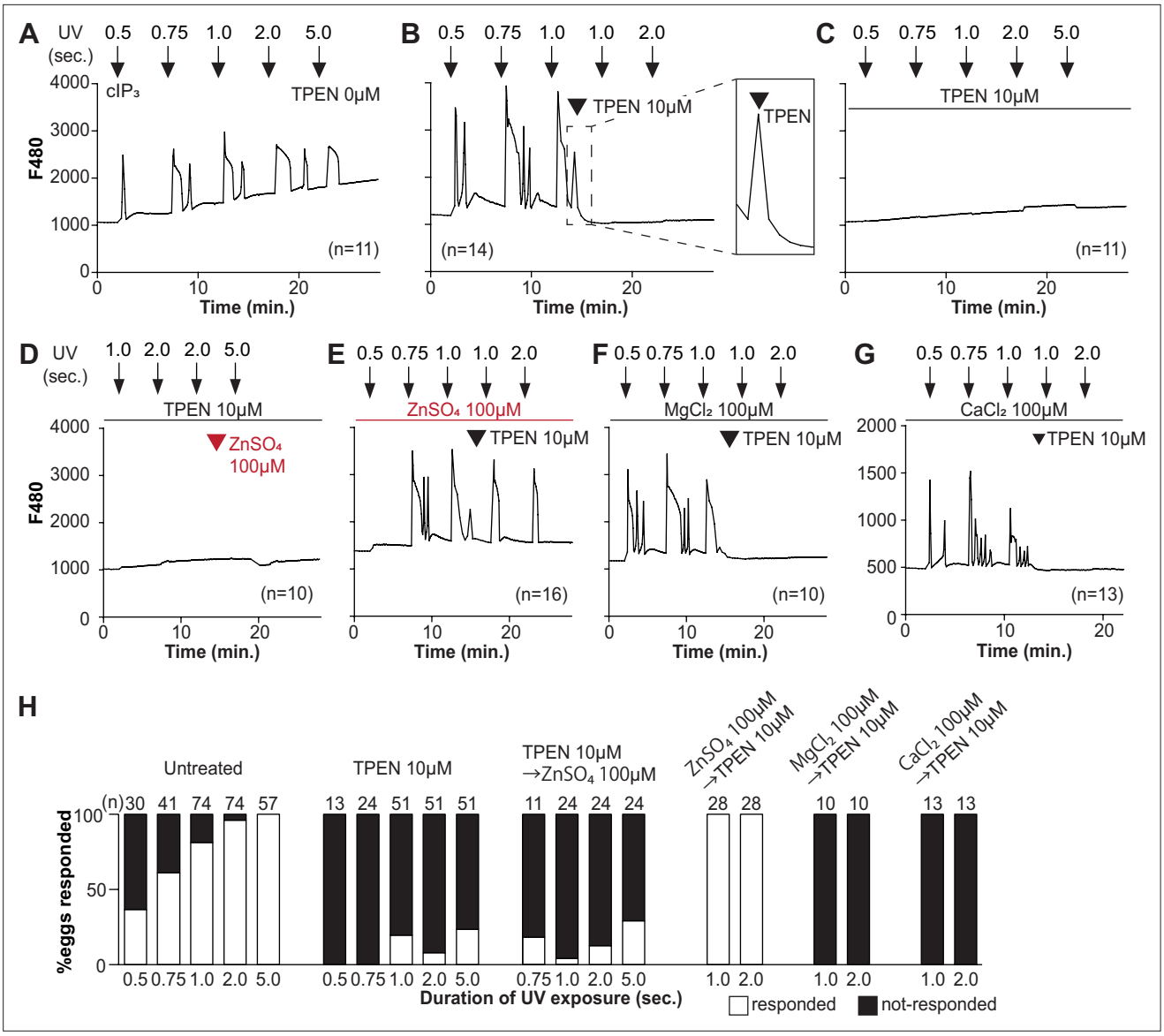

Figure 3. TPEN inhibition of cIP_3-induced Ca^{2+} release is precluded by $ZnSO_4$ supplementation before TPEN exposure. (**A–G**) Representative Ca^{2+} responses in MII eggs triggered by the release of caged IP_3 (cIP_3) induced by UV light pulses of increasing duration (arrows). (**A**) A representative control trace without TPEN, and (**B**) following the addition of 10 μM TPEN between the third and the fourth pulses. The broken line rectangle is magnified in the inset, farthest right side of the panel displaying the near immediate termination of an ongoing rise. (**C, D**) Recordings started in the presence of 10 μM TPEN but in (**D**) 100 μM $ZnSO_4$ was added between the second and the third pulses. (**E**) Recording started in the presence of 100 μM $ZnSO_4$ followed by the addition of 10 μM TPEN between the third and the fourth pulses. (**F, G**) Recording started in the presence of 100 μM $MgSO_4$ (**F**) or 100 μM $CaCl_2$ (**G**) and 10 μM TPEN added as above. Arrowheads above the different panels indicate the time of TPEN or divalent cation addition. (**H**) Bar graphs summarizing the number and percentages of eggs that responded to a given duration of UV pulses under each of the TPEN ± divalent ions.

The online version of this article includes the following figure supplement(s) for figure 3:

Figure supplement 1. Overexpression of endoplasmic reticulum (ER) accessory protein ERp44 did not change the Ca^{2+} responses initiated by m*Plcz1* mRNA microinjection, acetylcholine, or $SrCl_2$.

supplement 1), and overexpression of ERp44 modified neither the Ca^{2+} oscillations induced by agonists (***Figure 3—figure supplement 1***) nor the effectiveness of TPEN to block them (data not shown). Thus, TPEN and Zn^{2+} deficiency most likely inhibits Ca^{2+} release by directly interfering with IP_3R1 function rather than modifying this particular regulator.

Zn^{2+} depletion diminishes the ER Ca^{2+} leak and increases Ca^{2+} store content

Our above cIP_3 results that TPEN inhibited IP_3R1-mediated Ca^{2+} release and interrupted in-progress Ca^{2+} rises despite the presence of high levels of environmental IP_3 suggest its actions are probably independent of IP_3 binding, agreeing with an earlier report showing that TPEN did not modify IP_3's affinity for the IP_3R (***Richardson and Taylor, 1993***). Additionally, the presence of a Zn^{2+}-binding motif near the C-term cytoplasmic domain of the IP_3R1's channel, which is known to influence agonist-induced IP_3R1 gating (***Fan et al., 2015***), led us to posit and examine that Zn^{2+} deficiency may be disturbing Ca^{2+} release to the cytosol and out of the ER. To probe this possibility, we queried if pretreatment with TPEN inhibited Ca^{2+} release through IP_3R1. We first used thapsigargin (Tg), a sarcoplasmic/ER Ca^{2+} ATPase pump inhibitor (***Thastrup et al., 1990***) that unmasks a constitutive Ca^{2+} leak out of the ER (***Lemos et al., 2021***); in eggs, we have demonstrated it is mediated at least in part by IP_3R1 (***Wakai et al., 2019***). Treatment with TPEN for 15 min slowed the Tg-induced Ca^{2+} leak into the cytosol, resulting in delayed and lowered amplitude Ca^{2+} responses (***Figure 4A***; $p<0.05$). To test whether the reduced response to Tg means that TPEN prevented the complete response of Tg, leaving a temporarily increased Ca^{2+} content in the ER, we added the Ca^{2+} ionophore ionomycin (Io), which empties all stores independently of IP_3Rs. Io-induced Ca^{2+} responses were 3.3-fold greater in TPEN-treated cells, supporting the view that TPEN interferes with the ER Ca^{2+} leak (***Figure 4A***; $p<0.05$). We further evaluated this concept using in vitro aged eggs that often display reduced Ca^{2+} store content than freshly collected counterparts (***Abbott et al., 1998***). After culturing eggs in the presence or absence of TPEN for 2 hr, we added Io during Ca^{2+} monitoring, which in TPEN-treated eggs induced bigger Ca^{2+} rises than in control eggs (***Figure 4B***; $p<0.05$). We confirmed that this effect was independent of IP_3R1 degradation because TPEN did not change IP_3R1 reactivity in unfertilized eggs (***Figure 4C***; $p<0.05$).

Next, we used the genetically encoded FRET sensor D1ER (***Palmer et al., 2004***) to assess the TPEN's effect on the ER's relative Ca^{2+} levels changes following the additions of Tg or Ach. TPEN was added 10 min before 10 μM Tg or 50 μM Ach, and we simultaneously monitored changes in cytosolic and intra-ER Ca^{2+} (***Figure 4D and E***). For the first 3 min, the Tg-induced decrease in Ca^{2+}-ER was similar between groups. However, while the drop in Ca^{2+} content continued in control eggs, in TPEN-treated eggs, it came to an abrupt halt, generating profound differences between the two groups (***Figure 4D***; $p<0.05$). TPEN had even more pronounced effects following the addition of Ach, leading to a reduced- and prematurely terminated Ca^{2+} release from the ER in treated eggs (***Figure 4E***; $p<0.05$).

Lastly, we sought to use a cellular model where low labile Zn^{2+} occurred without pharmacology. To this end, we examined a genetic model where the two non-selective plasma membrane channels that could influx Zn^{2+} in maturing oocytes have been deleted (***Bernhardt et al., 2017***; ***Carvacho et al., 2016***; ***Carvacho et al., 2013***), namely, the transient receptor potential melastatin-7 (TRPM7) and TRP vanilloid 3 (TRPV3), both members of the TRP superfamily of channels (***Wu et al., 2010***). We found that eggs from double knockout females (dKOs) had lower levels of labile Zn^{2+} (***Figure 4F***), and the addition of Tg revealed an expanded Ca^{2+} store content in these eggs vs. control WT eggs (***Figure 4G***). Remarkably, in dKO eggs, the Ca^{2+} rise induced by Tg showed a shoulder or inflection point before the peak delaying the time to peak (***Figure 4G***, inset; $p<0.001$). These results in dKO eggs show a changed dynamic of the Tg-induced Ca^{2+} release, suggesting that lower levels of labile Zn^{2+} modify ER Ca^{2+} release independently of chelators.

Ca^{2+} oscillations in eggs occur within a window of Zn^{2+} concentrations

We next examined whether resupplying Zn^{2+} could restart the Ca^{2+} oscillations terminated by Zn^{2+} depletion. Zn pyrithione (ZnPT) rapidly increases cellular Zn^{2+} upon extracellular addition (***Barnett et al., 1977***; ***Robinson, 1964***). Dose titration studies and imaging fluorimetry revealed that 0.01 μM ZnPT caused subtle and protracted increases in Zn^{2+} levels, whereas 0.1 μM ZnPT caused rapid increases in eggs' Zn^{2+} baseline (***Figure 5A***). We induced detectable Ca^{2+} oscillations by injection of m*Plcz1* mRNA followed by 50 μM TPEN (***Figure 5B***), which terminated them. After 30 min, we added 0.1 μM ZnPT, and within 15 min the oscillations restarted in most TPEN-treated eggs (***Figure 5C***). We repeated this approach using thimerosal (***Figure 5D and E***). Adding 0.1 μM ZnPT did not restore the

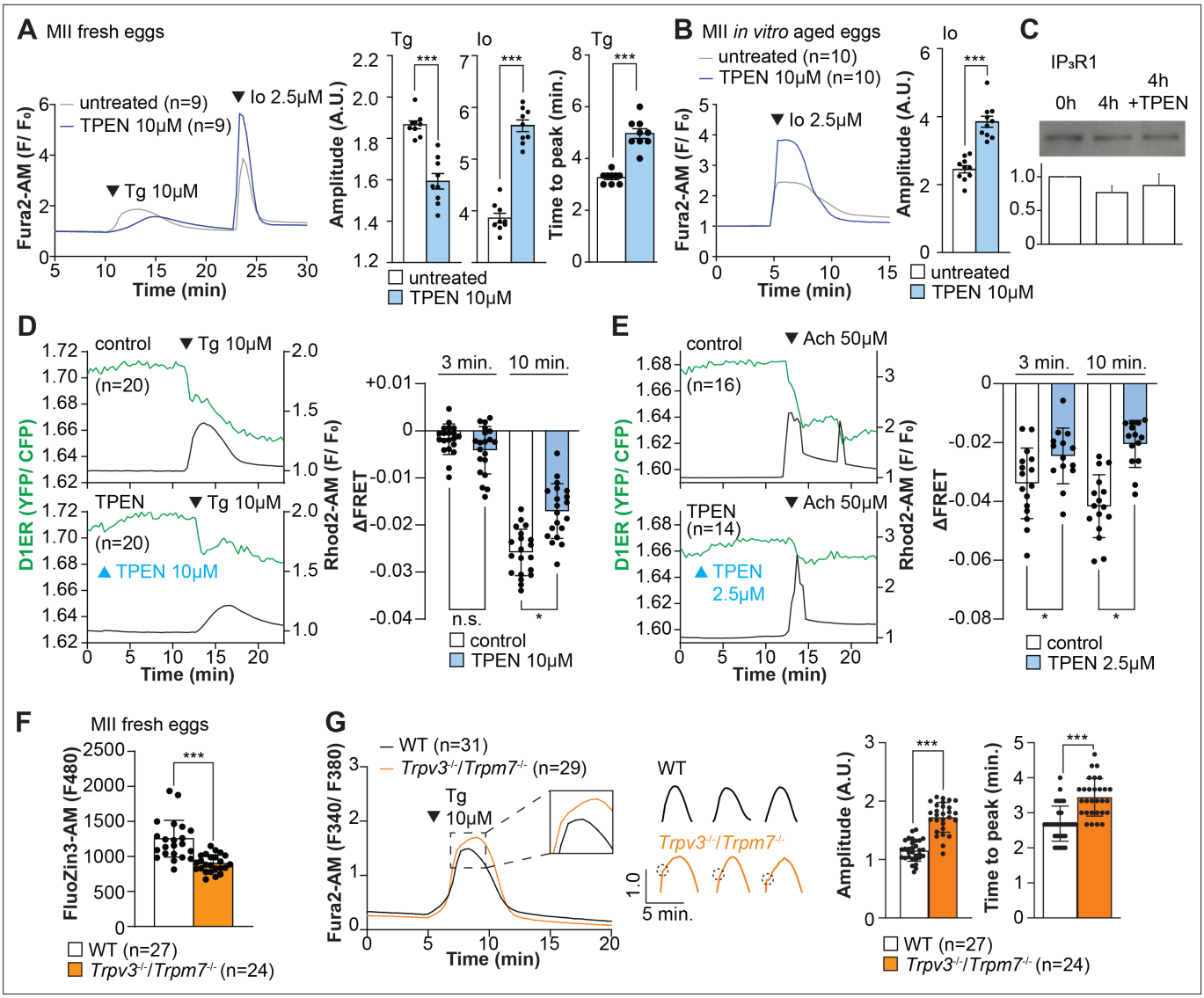

Figure 4. Zn^{2+} depletion alters Ca^{2+} homeostasis and increases Ca^{2+} store content independent of IP_3R1 mass. (**A, B**) Representative Ca^{2+} traces of MII eggs after the addition of Tg and Io in the presence or absence of TPEN. Blue trace recordings represent TPEN-treated eggs, whereas gray traces represent control, untreated eggs. (**A**) Io was added to fresh MII eggs once Ca^{2+} returned to baseline after treatment with Tg. Comparisons of mean peak amplitudes after Tg and Io are shown in the bar graphs in the right panel ($p<0.001$). (**B**) MII eggs were aged by 2 hr. incubation supplemented or not with TPEN followed by Io addition and Ca^{2+} monitoring ($p<0.001$). (**C**) Western blot showing the intensities of IP_3R1 bands in MII eggs freshly collected, aged by 4 hr. incubation without TPEN, and with TPEN. Thirty eggs per lane in all cases. This experiment was repeated three times. (**D, E**) Left panels: representative traces of Ca^{2+} values in eggs loaded with the Ca^{2+}-sensitive dye Rhod-2 AM and the ER Ca^{2+}reporter, D1ER (1 μg/μl mRNA). TPEN was added into the media followed 10 min later by (**D**) 10 μM Tg and (**E**) 50 μM Ach. Right panel: bars represent the difference of FRET value between at the time of Tg/ Ach addition and at 3 and 5 min later of the addition ($p<0.05$). Experiments were repeated two different times for each treatment. Black and green traces represent cytosolic Ca^{2+} and Ca^{2+}-ER, respectively. Blue and black arrowheads indicate the time of addition of TPEN and Tg/ Ach, respectively. (**F**) Basal Zn^{2+} level comparison in WT (open bar) and *Trpv3*$^{-/-}$/*Trpm7*$^{-/-}$ (dKO, orange bar) MII eggs. Each plot represents the Fluozin3 measurement at 5 min after starting monitoring. (**G**) Left panel: representative Ca^{2+} traces of WT (black trace) and dKO (orange trace) MII eggs after adding Tg. Insets represent the magnified traces at the peak of Ca^{2+} spike from different sets of eggs. Middle panel: individual traces of WT and dKO eggs after Tg addition. Dashed circles represent the flection point in dKO traces. Right panel: comparisons of mean peak amplitudes after Tg and the time between Tg addition and the Ca^{2+} peak are shown in the bar graphs in the right panel ($p<0.001$).

The online version of this article includes the following source data for figure 4:

Source data 1. IP_3R1 and TPEN western blotting.

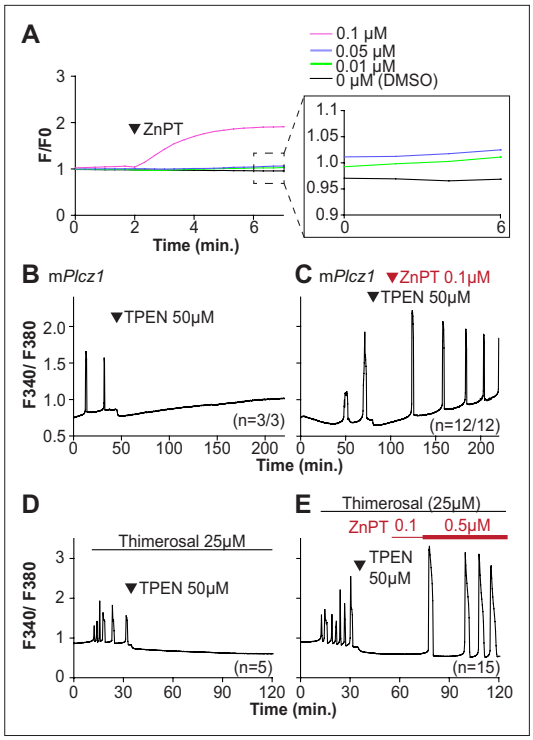

Figure 5. Restoring Zn^{2+} levels with ZnPT rescues oscillations interrupted by TPEN-induced Zn^{2+} deficiency. (**A**) Representative traces of Zn^{2+} in MII eggs following the addition of 0.01–0.1 μM concentrations of ZnPT. The broken rectangular area is amplified in the next panel to appreciate the subtle increase in basal Zn^{2+} caused by the addition of ZnPT. (**B, C**) m*Plcz1* mRNA (0.01 μg/μl)-induced oscillations followed by the addition of TPEN (black arrowhead) (**B**), or after the addition of TPEN followed by ZnPT (red arrowhead) (**C**). (**D, E**) Thimerosal (25 μM) induced oscillations using the same sequence of TPEN (**D**) and ZnPT (**E**), but higher concentrations of ZnPT were required to rescue thimerosal-initiated oscillations (**E**). These experiments were repeated at least two different times.

Ca^{2+} oscillations retrained by TPEN, but 0.5 μM ZnPT did so (***Figure 5E***). These results demonstrate that Zn^{2+} plays a pivotal, enabling role in the generation of Ca^{2+} oscillations in mouse eggs.

Excessive intracellular Zn^{2+} inhibits Ca^{2+} oscillations

Zn^{2+} is necessary for diverse cellular functions, consistent with numerous amino acids and proteins capable of binding Zn^{2+} within specific and physiological ranges (***Pace and Weerapana, 2014***). Excessive Zn^{2+}, however, can cause detrimental effects on cells and organisms (***Broun et al., 1990***; ***Hara et al., 2022***; ***Sikora and Ouagazzal, 2021***). Consistent with the deleterious effects of Zn^{2+}, a previous study showed that high concentrations of ZnPT, ~50 μM, prevented $SrCl_2$-induced egg activation and initiation of development (***Bernhardt et al., 2012***; ***Kim et al., 2011***). We examined how ZnPT and excessive Zn^{2+} levels influence Ca^{2+} oscillations. Our conditions revealed that pre-incubation or continuous exposure to 0.1 μM or 1.0 μM ZnPT delayed or prevented egg activation induced by m*Plcz1* mRNA injection (***Figure 6—figure supplement 1***). We used these ZnPT concentrations to add it into ongoing oscillations induced by ICSI and monitored the succeeding Ca^{2+} responses. The addition of 0.05–10 μM ZnPT caused an immediate elevation of the basal levels of Fura-2 and termination of the Ca^{2+} oscillations (***Figure 6A–D***). m*Plcz1* mRNA-initiated Ca^{2+} responses were also interrupted by adding 0.1 μM ZnPT, whereas untreated eggs continued oscillating (***Figure 6E and F***). ZnPT also inhibited IP_3R1-mediated Ca^{2+} release triggered by cIP_3, suggesting that excessive Zn^{2+} directly inhibits IP_3R1 function (***Figure 6G***).

A noticeable feature of ZnPT is the increased basal ratios of Fura-2 AM. These changes could reflect enhanced IP_3R1 function and increased basal Ca^{2+} concentrations caused by Zn^{2+} stimulation of IP_3R1. This seems unlikely, however, because extended elevated cytosolic Ca^{2+} would probably induce cellular responses, such as the release of the second polar body, egg fragmentation, or cell death, neither of which happened. It might reflect, instead, Fura-2's ability to report changes in Zn^{2+} levels, which seemed the case because the addition of TPEN lowered fluorescence without restarting the Ca^{2+} oscillations (***Figure 6F***). To ensure the impact of ZnPT abolishing Ca^{2+} oscillations was not an imaging artifact obscuring ongoing rises, we simultaneously monitored cytoplasmic and ER Ca^{2+} levels with Rhod-2 and D1ER, respectively. This approach allowed synchronously observing Ca^{2+} changes in both compartments that should unfold in opposite directions. In control, uninjected eggs, the fluorescent values for both reporters remained unchanged during the monitoring period, whereas in m*Plcz1* mRNA-injected eggs, the reporters' signals displayed simultaneous but opposite changes, as expected (***Figure 6H and I***). The addition of ZnPT in uninjected eggs rapidly increased Rhod-2 signals but not D1ER's, which was also the case in oscillating eggs, as the addition of ZnPT did not immediately alter the dynamics of the ER's Ca^{2+} release, suggesting that D1ER faithfully reports in Ca^{2+} changes but cannot detect changes in Zn^{2+} levels, at least to this extent; ZnPT progressively caused fewer and lower amplitude changes

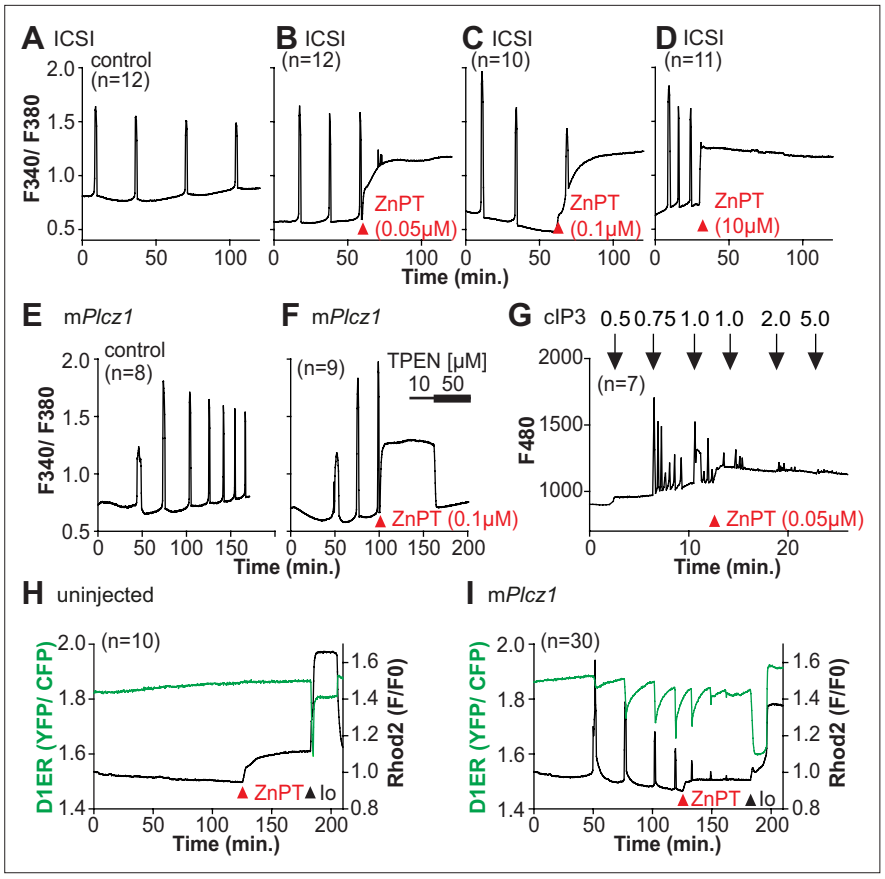

Figure 6. Excess Zn^{2+} hinders Ca^{2+} oscillations. (**A–D**) Intracytoplasmic sperm injection (ICSI)-initiated Ca^{2+} response without (**A**) or following the addition of ZnPT (**B, C**) (the time of ZnPT addition and concentration are denoted above the tracing). (**E, F**) Representative Ca^{2+} responses induced by injection of 0.01 μg/μl m*Plcz1* mRNA in untreated eggs (**E**) or in eggs treated with 0.1 μM ZnPT followed by 10 μM TPEN first and then 50 μM (**F**). (**G**) cIP_3-induced Ca^{2+} release as expected when the UV pulses in the absence but not in the presence of 0.05 μM ZnPT (the time of addition is denoted by a bar above the tracing). (**H, I**) Representative traces of Ca^{2+} values in eggs loaded with the Ca^{2+}-sensitive dye Rhod-2 AM and the ER Ca^{2+}reporter, D1ER (1 μg/μl mRNA). Uninjected and 0.01 μg/μl m*Plcz1* mRNA-injected eggs were monitored. After initiation and establishment of the oscillations, 0.1 μM ZnPT was added into the media followed 30 min later by 2.5 μM Io. Experiments were repeated two different times. Red and black arrowheads indicate the time of addition of ZnPT and Io, respectively.

The online version of this article includes the following figure supplement(s) for figure 6:

Figure supplement 1. Elevated Zn^{2+} impairs egg activation and the subsequent embryo development.

in D1ER fluorescence, consistent with the diminishing and eventual termination of the Ca^{2+} oscillations. Noteworthy, in these eggs, the basal D1ER fluorescent ratio remained unchanged after ZnPT, demonstrating its unresponsiveness to Zn^{2+} changes of this magnitude. The ZnPT-induced increases in Rhod-2 fluorescence without concomitant changes in D1ER values suggest that the changes in the dyes' fluorescence do not represent an increase in basal Ca^{2+} and, more likely, signal an increase in intracellular Zn^{2+}. We confirmed that both reporters were still in working order as the addition of Io triggered Ca^{2+} changes detected by both reporters (***Figure 6H and I***).

Discussion

This study demonstrates that appropriate levels of labile Zn^{2+} are essential for initiating and maintaining IP_3R1-mediated Ca^{2+} oscillations in mouse eggs regardless of the initiating stimuli. Both deficient and excessive Zn^{2+} compromise IP_3R1 sensitivity, diminishing and mostly terminating Ca^{2+} oscillations. The results demonstrate that IP_3R1 and Zn^{2+} act in concert to modulate Ca^{2+} signals, revealing previously unexplored crosstalk between these ions at fertilization (***Figure 7***).

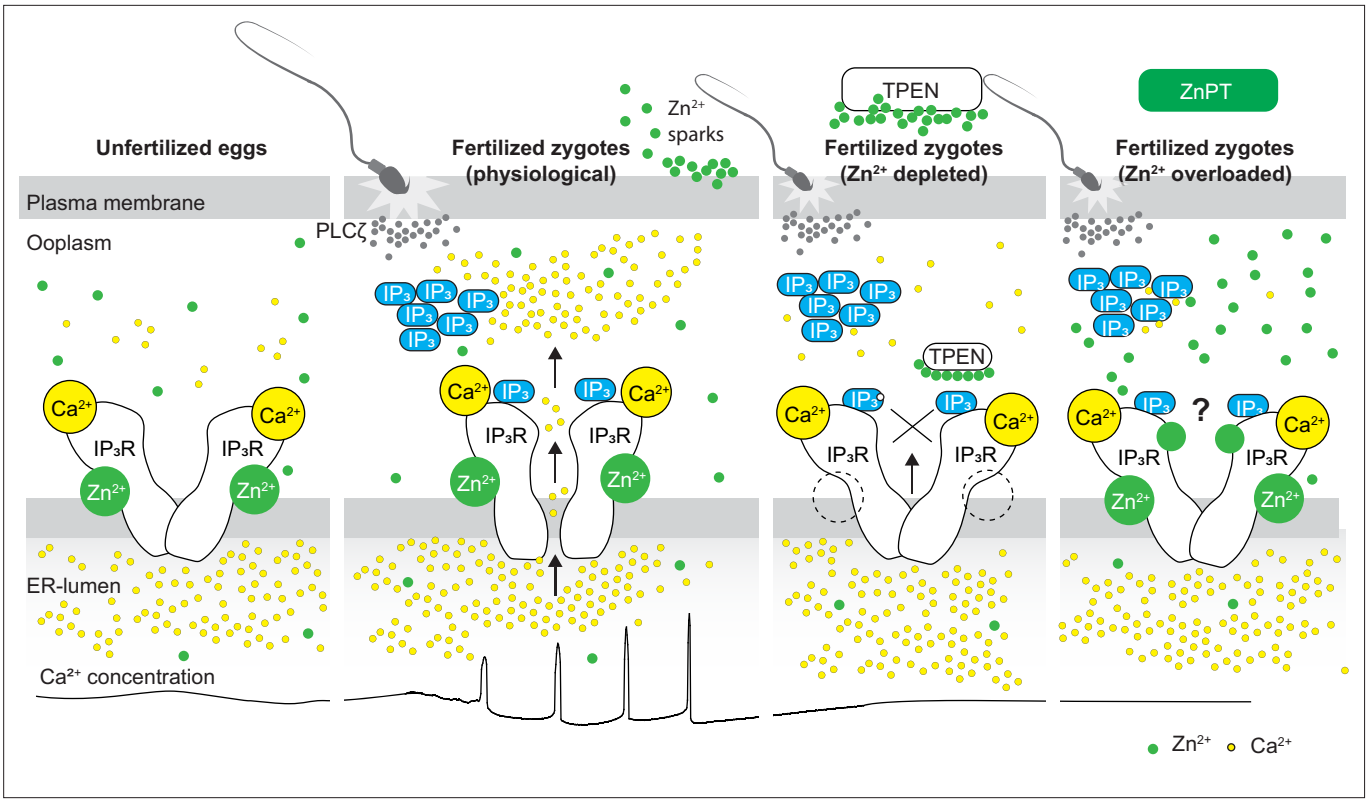

Figure 7. Schematic of proposed regulation of IP_3R1 function by Zn^{2+} in eggs and fertilized zygotes. In MII eggs, left panel, IP_3R1s are in a Ca^{2+}-release permissive state with optimal levels of cytoplasmic Ca^{2+} and Zn^{2+} and maximum endoplasmic reticulum (ER) content, but Ca^{2+} is maintained at resting levels by the combined actions of pumps, ER Ca^{2+} leak, and reduced influx. Once fertilization takes place, left center panel, robust IP_3 production induced by the sperm-borne PLC ζ leads to Ca^{2+} release through ligand-induced gating of IP_3R1. Continuous IP_3 production and refilling of the stores via Ca^{2+} influx ensure the persistence of the oscillations. Zn^{2+} release occurs in association with first few Ca^{2+} rises and cortical granule exocytosis, Zn^{2+} sparks, lowering Zn^{2+} levels but not sufficiently to inhibit IP_3R1 function. Zn^{2+} deficiency caused by TPEN or other permeable Zn^{2+} chelators, right center panel, dose-dependently impairs IP_3R1 function and limits Ca^{2+} release. We propose this is accomplished by stripping the Zn^{2+} bound to the residues of the zinc-finger motif in the LNK domain of IP_3R1 that prevents the allosteric modulation of the gating process induced by IP_3 or other agonists. We propose that excess Zn^{2+}, right panel, also inhibits IP_3R1-mediate Ca^{2+} release, possibly by non-specific binding of thiol groups present in cysteine residues throughout the receptor (denoted by a?). We submit that optimal Ca^{2+} oscillations in mouse eggs unfold in the presence of a permissive range of Zn^{2+} concentration.

Zn^{2+} is an essential micronutrient for living organisms (***Kaur et al., 2014***) and is required for various cellular functions, such as proliferation, transcription, and metabolism (***Lo et al., 2020***; ***Maret and Li, 2009***; ***Yamasaki et al., 2007***). Studies using Zn^{2+} chelators have uncovered what appears to be a cell-specific, narrow window of Zn^{2+} concentrations needed for cellular proliferation and survival (***Carraway and Dobner, 2012***; ***Lo et al., 2020***). Further, TPEN appeared especially harmful, and in a few cell lines, even low doses provoked oxidative stress, DNA fragmentation, and apoptosis (***Mendivil-Perez et al., 2012***). We show here that none of the Zn^{2+} chelators, permeable or impermeable, affected cell viability within our experimental observations, confirming findings from previous studies that employed high concentrations of TPEN to interrupt the Ca^{2+} oscillations (***Lawrence et al., 1998***) or inducing egg activation of mouse eggs (***Suzuki et al., 2010b***). Our data demonstrating that ~2.5 μM is the threshold concentration of TPEN in eggs that first causes noticeable changes in basal Zn^{2+}, as revealed by FluoZin, is consistent with the ~2–5 μM Zn^{2+} concentrations in most culture media without serum supplementation (***Lo et al., 2020***), and with the ~100 pM basal Zn^{2+} in cells (***Qin et al., 2011***). Lastly, the effects on Ca^{2+} release observed here with TPEN and other chelators were due to the chelation of Zn^{2+}, as pretreatment with $ZnSO_4$ but not with equal or greater concentrations of $MgCl_2$ or $CaCl_2$ rescued the inhibition of the responses, which is consistent with results by others (***Kim et al., 2010***; ***Lawrence et al., 1998***).

To identify how Zn^{2+} deficiency inhibits Ca^{2+} release in eggs, we induced Ca^{2+} oscillations using various stimuli and tested the effectiveness of membrane-permeable and -impermeable chelators to abrogate them. Chelation of extracellular Zn^{2+} failed to terminate the Ca^{2+} responses, whereas membrane-permeable chelators did, pointing to intracellular labile Zn^{2+} levels as essential for Ca^{2+} release. All agonists used here were susceptible to inhibition by TPEN, whether their activities depended on IP_3 production or allosterically induced receptor function, although the effective TPEN concentrations varied across stimuli. Some agents, such as m*Plcz1* mRNA or thimerosal, required higher concentrations than $SrCl_2$, Ach, or cIP_3. The reason underlying the different agonists' sensitivities to TPEN will require additional research, but the persistence of IP_3 production or change in IP_3R1 structure needed to induce channel gating might explain it. However, the universal abrogation of Ca^{2+} oscillations by TPEN supports the view drawn from cryo-EM-derived IP_3R1 models that signaling molecules can allosterically induce channel gating from different starting positions in the receptor by mechanically coupling the binding effect to the ion-conducting pore in the C-terminal end of IP_3R (***Fan et al., 2015***). The cytosolic C-terminal domain of each IP_3R1 subunit is alongside the IP_3-binding domain of another subunit and, therefore, well positioned to sense IP_3 binding and induce channel gating (***Fan et al., 2015***). Within each subunit, the LNK domain, which contains a Zn^{2+}-finger motif (***Fan et al., 2015***), connects the opposite domains of the molecule. Although there are no reports regarding the regulation of IP_3R1 sensitivity by Zn^{2+}, such evidence exists for RyRs (***Woodier et al., 2015***), which also display a conserved Zn^{2+}-finger motif (***des Georges et al., 2016***). Lastly, mutations of the two Cys or two His residues of this motif, without exception, resulted in inhibition or inactivation of the IP_3R1 channel (***Bhanumathy et al., 2012***; ***Uchida et al., 2003***). These results are consistent with the view that the C-terminal end of IP_3Rs plays a dominant role in channel gating (***Bhanumathy et al., 2012***; ***Uchida et al., 2003***). We propose that TPEN inhibits Ca^{2+} oscillations in mouse eggs because chelating Zn^{2+} interferes with the function of the LNK domain and its Zn^{2+}-finger motif proposed role on the mechanical coupling induced by agonist binding to the receptor that propagates to the pore-forming region and required to gate the channel's ion-pore (***Fan et al., 2022***; ***Fan et al., 2015***).

In support of this possibility, TPEN-induced Zn^{2+}-deficient conditions altered the Ca^{2+}-releasing kinetics in resting eggs or after fertilization. Tg increases intracellular Ca^{2+} by inhibiting the SERCA pump (***Thastrup et al., 1990***) and preventing the reuptake into the ER of the ebbing Ca^{2+} during the basal leak. Our previous studies showed that the downregulation of IP_3R1 diminishes the leak, suggesting that it occurs through IP_3R1 (***Wakai and Fissore, 2019***). Consistent with this view, TPEN pretreatment delayed the Ca^{2+} response induced by Tg, implying that Zn^{2+} deficiency hinders Ca^{2+} release through IP_3R1. An expected consequence would be increased Ca^{2+} content in the ER after Tg. Io that mobilizes Ca^{2+} independently of IP_3Rs (***Toeplitz et al., 1979***) induced enhanced responses in TPEN-treated eggs vs. controls, confirming the accumulation of Ca^{2+}- ER in Zn^{2+}-deficient conditions. We demonstrated that this accumulation is due to hindered emptying of the Ca^{2+} ER evoked by agonists in Zn^{2+}-deficient environments, resulting in reduced cytosolic Ca^{2+} increases, as IP_3R1 is the pivotal intermediary channel between these compartments. Noteworthy, the initial phase of the Tg-induced Ca^{2+} release out of the ER did not appear modified by TPEN, as if it was mediated by a Zn^{2+}-insensitive Ca^{2+} channel(s)/transporter, contrasting with the abrogation of Ach-induced ER emptying from the outset. Remarkably, independently of Zn^{2+} chelators, emptying of Ca^{2+} ER was modified in a genetic model of Zn^{2+}-deficient oocytes lacking two TRP channels, confirming the impact of Zn^{2+} on Ca^{2+} release. It is worth noting that TPEN did not reduce but maintained or increased the mass of IP_3R1, which might result in the inhibition of Zn^{2+}-dependent ubiquitin ligase Ubc7 by the Zn-deficient conditions (***Webster et al., 2003***). We cannot rule out that these conditions may undermine other conformational changes required to trigger IP_3R1 degradation, thereby favoring the accumulation of IP_3R1.

Despite accruing Zn^{2+} during oocyte maturation, fertilization witnesses a necessary Zn^{2+} release into the external milieu, known as 'Zn^{2+} sparks' (***Converse and Thomas, 2020***; ***Kim et al., 2011***; ***Mendoza et al., 2022***; ***Que et al., 2019***; ***Que et al., 2015***; ***Seeler et al., 2021***). This release of Zn^{2+} is a conserved event in fertilization across species and is associated with several biological functions, including those related to fending off polyspermy (***Kim et al., 2011***; ***Que et al., 2019***; ***Wozniak et al., 2020***). The concomitant decrease in Zn^{2+} facilitates the resumption of the cell cycle and exit from the MII stage (***Kim et al., 2011***). Congruent with this observation, artificial manipulation that maintains high Zn^{2+} levels prevents egg activation (***Kim et al., 2011***), whereas lowering Zn^{2+} with

chelators leads to egg activation without Ca^{2+} mobilization (***Suzuki et al., 2010b***). As posed by others, these results suggest that meiosis completion and the early stages of fertilization unfold within a narrow window of permissible Zn^{2+} (***Kim et al., 2011***; ***Kim et al., 2010***). Here, we extend this concept and show that IP_3R1 function and the Ca^{2+} oscillations in mouse eggs require this optimal level of labile Zn^{2+} because the Ca^{2+} responses interrupted by TPEN-induced Zn^{2+}-insufficiency are rescued by restoring Zn^{2+} levels with ZnPT. Furthermore, unopposed increases in Zn^{2+} by exposure to ZnPT abrogated fertilization-initiated Ca^{2+} oscillations and prevented the expected egg activation events. It is unclear how excess Zn^{2+} disturbs the function of IP_3R1. Nevertheless, IP_3R1s have multiple cysteines whose oxidation enhances the receptor sensitivity to IP_3 (***Joseph et al., 2018***), and it is possible that excessive Zn^{2+} aberrantly modifies them, disturbing IP_3R1 structure and function or, alternatively, preventing their oxidation and sensitization of the receptor. Lastly, we cannot rule out that high Zn^{2+} levels directly inhibit the receptor's channel. These results reveal a close association between the Zn^{2+} levels controlling meiotic transitions and the Ca^{2+} release necessary for egg activation, placing the IP_3R1 at the center of the crosstalk of these two divalent cations.

Abrupt Zn^{2+} changes have emerged as critical signals for meiotic and mitotic transitions in oocytes, eggs, embryos, and somatic cells (***Kim et al., 2011***; ***Kim et al., 2010***; ***Lo et al., 2020***). Fertilization relies on prototypical Ca^{2+} rises and oscillations, and Zn^{2+} sparks are an egg activation event downstream of this Ca^{2+} release, establishing a functional association between these two divalent cations that continues to grow (***Kim et al., 2011***). Here, we show that, in addition, these cations actively crosstalk during fertilization and that the fertilization-induced Ca^{2+} oscillations rely on optimized IP_3R1 function underpinned by ideal Zn^{2+} levels set during oocyte maturation. Future studies should explore if artificial alteration of Zn^{2+} levels can extend the fertile lifespan of eggs, improve developmental competence, or develop methods of non-hormonal contraception.

Materials and methods

Key resources table

Reagent type (species) or resource	Designation	Source or reference	Identifiers	Additional information
Genetic reagent (*Mus musculus*)	CD1	Charles River	022	
Genetic reagent (*M. musculus*)	C57BL/6J	JAX	JAX: 000664	
Genetic reagent (*M. musculus*)	*Trpm7*-floxed	A generous gift from Dr. Carmen P. Williams (NIEHS) (PMID:30322909)		C57BL6/J and 129s4/SvJae mixed background
Genetic reagent (*M. musculus*)	*Gdf9-cre*	JAX	JAX: 011062	
Genetic reagent (*M. musculus*)	*Trpv3*$^{-/-}$	A generous gift from Dr H. Xu (PMID:20403327)		C57BL/6J and 129/SvEv mixed background
Biological sample (mouse oocyte)	*Mus musculus*	This paper		Eggs at the metaphase of the second meiosis
Biological sample (mouse sperm)	*Mus musculus*	This paper		Matured sperm from cauda epididymis
Recombinant DNA reagent	pcDNA6-mouse *Plcz1-venus* (plasmid used as a template for mRNA synthesis)	Published in previous Fissore lab paper PMID: 34313315 Mouse *Plcz1* sequence was a generous gift from Dr. Kiyoko Fukami (PMID:18028898)		Mouse *Plcz1* mRNA was fused with Venus and inserted in pcDNA6 vector
Recombinant DNA reagent	pcDNA6-CALR-D1ER-KDEL (plasmid used as a template for mRNA synthesis)	Published in previous Fissore lab paper PMID:24101727 Original D1ER vector was a generous gift from Dr. Roger Y Tsien (PMID:15585581)		FRET construct D1ER was inserted between ER-targeting sequence of calreticulin and KDEL ER retention signal in pcDNA6 vector

Continued on next page

Continued

Reagent type (species) or resource	Designation	Source or reference	Identifiers	Additional information
Recombinant DNA reagent	pcDNA6-human *ERP44-HA* (plasmid used as a template for mRNA synthesis)	This paper Original human ERp44 sequence was a generous gift from Dr. Roberto Sitia (PMID:11847130)		Human *ERP44* mRNA fused with HA in pcDNA6/Myc His B vector
Antibody	Monoclonal HA (mouse monoclonal)	Roche	11581816001	Dilution: 1:200
Antibody	Polyclonal IP_3R1 (rabbit polyclonal)	***Parys et al., 1995***		Dilution: 1:1000
Antibody	Monoclonal α-tubulin (mouse monoclonal)	Sigma-Aldrich	T-9026	Dilution: 1:1000
Antibody	Alexa Fluor 488 (goat polyclonal)	Invitrogen	Invitrogen: A32723	Dilution: 1:400
Commercial assay or kit	T7 mMESSAGE mMACHINE Kit	Invitrogen	Invitrogen: AM1344	Used for in vitro mRNA synthesis
Commercial assay or kit	Poly(A) Tailing Kit	Invitrogen	Invitrogen: AM1350	Used for poly (A) tailing of synthesized mRNA
Chemical compound, drug	Hyaluronidase from bovine testes	Sigma-Aldrich	H3506	
Chemical compound, drug	3-Isobutyl-1-methylxanthine (IBMX)	Sigma-Aldrich	I5879	
Chemical compound, drug	Polyvinylpyrrolidone (PVP) (average molecular weight: 360,000)	Sigma-Aldrich	PVP360	Used for mRNA microinjection and ICSI
Chemical compound, drug	N,N, N′,N′-Tetrakis (2-pyridylmethyl) ethylenediamine (TPEN)	Sigma-Aldrich	P4413	Prepared in DMSO and kept at –20°C until use
Chemical compound, drug	Zinc pyrithione (ZnPT)	Sigma-Aldrich	PHR1401	Prepared in DMSO and kept at –20°C until use
Chemical compound, drug	Strontium chloride hexahydrate ($SrCl_2$)	Sigma-Aldrich	255521	Freshly dissolved in water on the day of experiment
Chemical compound, drug	Calcium chloride dihydrate ($CaCl_2$)	Sigma-Aldrich	C3881	Freshly dissolved in water on the day of experiment
Chemical compound, drug	Magnesium chloride hexahydrate ($MgCl_2$)	Sigma-Aldrich	M2393	Freshly dissolved in water on the day of experiment
Chemical compound, drug	Zinc sulfate monohydrate ($ZnSO_4$)	Acros Organics	389802500	Freshly dissolved in water on the day of experiment
Chemical compound, drug	Ethylenediaminetetraacetic acid sodium dihydrate (EDTA)	LabChem	LC137501	Prepared as 0.5 M aqueous solution with pH 8.0 adjusted by NaOH
Chemical compound, drug	Diethylenetriaminepentaacetic acid (DTPA)	Sigma-Aldrich	D6518	
Chemical compound, drug	Tris (2-pyridylmethyl) amine (TPA)	Santa Cruz	sc-477037	
Chemical compound, drug	Dimethyl sulfoxide (DMSO)	Sigma-Aldrich	D8418	Used as a solvent
Chemical compound, drug	Acetylcholine chloride	Sigma-Aldrich	A6625	
Chemical compound, drug	Thimerosal	Sigma-Aldrich	T5125	Freshly dissolved in water on the day of experiment and kept on ice until use

Continued on next page

Continued

Reagent type (species) or resource	Designation	Source or reference	Identifiers	Additional information
Chemical compound, drug	Ionomycin calcium salt	Tocris	1704	Working concentration: 2.5 µM
Chemical compound, drug	Thapsigargin	Calbiochem	#586500	Working concentration: 10 µM
Other	Pluronic F-127 (20% solution in DMSO) (pluronic acid)	Invitrogen	P3000MP	Added to dye dilutions to facilitate the solubilization
Other	Fura-2 AM	Invitrogen	F1221	Ratiometric fluorescent Ca^{2+} indicator Used at 1.25 µM in TL-HEPES containing 0.02% pluronic acid
Other	FluoZin-3 AM	Invitrogen	F24195	Fluorescent Zn^{2+} indicator Used at 1.25 µM in TL-HEPES containing 0.02% pluronic acid
Other	Fluo-4 AM	Invitrogen	F14201	Fluorescent Ca^{2+} indicator Used at 1.25 µM in TL-HEPES containing 0.02% pluronic acid
Other	Rhod2-AM	Invitrogen	R1244	Fluorescent Ca^{2+} indicator Used at 2.2 µM in TL-HEPES containing 0.02% pluronic acid.
Other	ci-IP3/PM	Tocris	6210	Photo-activatable IP_3. Dissolved in DMSO and kept at –20°C Before use, the stock was diluted with water to make a final concentration of 0.25 mM
Other	Pme1	New England BioLabs	R0560S	Used to linearize pcDNA6 vectors for mRNA synthesis
Software, algorithm	Prism	GraphPad Software		Version 5.01

N,N,N′,N′-tetrakis (2-pyridinylmethyl)–1,2-ethylenediamine (TPEN) and zinc pyrithione (ZnPT) were dissolved in dimethyl sulfoxide (DMSO) at 10 mM and stored at –20°C until use. $SrCl_2$, $CaCl_2$, $ZnSO_4$, and $MgCl_2$ were freshly dissolved with double-sterile water at 1 M and diluted with the monitoring media just before use. Ethylenediaminetetraacetic acid (EDTA) and diethylenetriaminepentaacetic acid (DTPA) were reconstituted with double-sterile water at 0.5 M and 10 mM, respectively, and the pH was adjusted to 8.0. Tris(2-pyridylmethyl) amine (TPA) was diluted in DMSO at 100 mM and stored at –20°C until use. Acetylcholine chloride and thimerosal were dissolved in double-sterile water at 550 mM and 100 mM, respectively. Acetylcholine was stored at –20°C until use, whereas thimerosal was made fresh in each experiment.

Mice

The University of Massachusetts Institutional Animal Care and Use Committee (IACUC) approved all animal experiments and protocols. *Trpm7*-floxed (*Trpm7*$^{fl/fl}$) *Gdf9-Cre* and *Trpv3*$^{-/-}$ mice were bred at our facility. *Trpm7*$^{fl/fl}$ mice were crossed with *Trpv3*$^{-/-}$ to generate *Trpm7*$^{fl/fl}$; *Trpv3*$^{-/-}$ mouse line. Female *Trpm7*$^{fl/fl}$; *Trpv3*$^{-/-}$ mice were crossed with *Trpm7*$^{fl/fl}$; *Trpv3*$^{-/-}$; *Gdf9-cre* male to generate females null for *Trpv3* and with oocyte-specific deletion for *Trpm7*. Ear clips from offspring were collected prior to weaning, and confirmation of genotype was performed after most experiments.

Egg collection

All gamete handling procedures are as previously reported by us (***Wakai et al., 2019***). MII eggs were collected from the ampulla of 6- to 8-week-old female mice. Females were superovulated via intraperitoneal injections of 5 IU pregnant mare serum gonadotropin (PMSG, Sigma, St. Louis, MO) and 5 IU human chorionic gonadotropin (hCG, sigma) at 48 hr interval. Cumulus-oocyte-complexes (COCs) were obtained 13.5 hr post-hCG injection by tearing the ampulla using forceps and needles in TL-HEPES medium. COCs were treated with 0.26% (w/v) of hyaluronidase at room temperature (RT) for 5 min to remove cumulus cells.

Intracytoplasmic sperm injection (ICSI)

ICSI was performed as previously reported by us (***Kurokawa and Fissore, 2003***) using described setup and micromanipulators (Narishige, Japan). Sperm from C57BL/6 or CD1 male mice (7–12 weeks old) were collected from the cauda epididymis in TL-HEPES medium, washed several times, heads separated from tails by sonication (XL2020; Heat Systems Inc, USA) for 5 s at 4°C. The sperm lysate was washed in TL-HEPES and diluted with 12% polyvinylpyrrolidone (PVP, MW = 360 kDa) to a final PVP concentration of 6%. A piezo micropipette-driving unit was used to deliver the sperm into the ooplasm (Primetech, Ibaraki, Japan); a few piezo-pulses were applied to puncture the eggs' plasma membrane following penetration of the zona pellucida. After ICSI, eggs were either used for Ca^{2+} monitoring or cultured in KSOM to evaluate activation and development at 36.5°C in a humidified atmosphere containing 5% CO_2.

Preparation and microinjection of mRNA

pcDNA6-m*Plcz1-mEGFP*, pcDNA6-CALR-D1ER-KDEL, and pcDNA6-*humanERp44-HA* were linearized with the restriction enzyme PmeI and in vitro transcribed using the T7 mMESSAGE mMACHINE Kit following procedures previously used in our laboratory (***Ardestani et al., 2020***). A poly(A) tail was added to the in vitro synthesized RNA (mRNA) using Tailing Kit followed by quantification and dilution to 0.5 µg/µl in nuclease-free water and stored at –80°C until use. Before microinjection, m*Plcz1*, D1ER, and *ERp44* mRNA were diluted to 0.01, 1.0, and 0.5 µg/µl, respectively, in nuclease-free water, heated at 95°C for 3 min followed by centrifugation at 13,400 × *g* for 10 min at 4°C. Cytoplasm injection of mRNA was performed under microscopy equipped with micromanipulators (Narishige, Japan). The zona pellucida and the plasma membrane of MII eggs were penetrated by applying small pulses generated by the piezo micromanipulator (Primetech). The preparation of the injection pipette was as for ICSI (***Kurokawa and Fissore, 2003***), but the diameter of the tip was ~1 µm.

Ca^{2+} and Zn^{2+} imaging

Before Ca^{2+} imaging, eggs were incubated in TL-HEPES containing 1.25 µM Fura2-AM, 1.25 µM FluoZin3-AM, or 2.2 µM Rhod2-AM and 0.02% pluronic acid for 20 min at RT and then washed. The fluorescent probe-loaded eggs were allowed to attach to the bottom of the glass dish (Mat-Tek Corp., Ashland, MA). Eggs were monitored simultaneously using an inverted microscope (Nikon, Melville, NY) outfitted for fluorescence measurements. Fura-2 AM, FluoZin3-AM, and Rhod2-AM fluorescence were excited with 340 nm and 380 nm, 480 nm, and 550 nm wavelengths, respectively, every 20 s, for different intervals according to the experimental design and as previously performed in the laboratory. The illumination was provided by a 75 W Xenon arc lamp and controlled by a filter wheel (Ludl Electronic Products Ltd, Hawthorne, NY). The emitted light above 510 nm was collected by a cooled Photometrics SenSys CCD camera (Roper Scientific, Tucson, AZ). Nikon Element software coordinated the filter wheel and data acquisition. The acquired data were saved and analyzed using Microsoft Excel and GraphPad using Prism software (***Ardestani et al., 2020***). For ***Figures 1A, 4A–C, 5A, and 6H–I***, values obtained from FluoZin3-AM, Fura2-AM, or Rhod2-AM recordings were divided by the average of the first five recordings for each treatment that was used as the F_0.

To estimate relative changes in Ca^{2+}-ER, emission ratio imaging of the D1ER (YFP/CFP) was performed using a CFP excitation filter, dichroic beamsplitter, CFP and YFP emission filters (Chroma Technology, Rockingham, VT; ET436/20X, 89007bs, ET480/40m, and ET535/30m). To measure Ca^{2+}-ER and cytosolic Ca^{2+} simultaneously, eggs that had been injected with D1ER were loaded with Rhod-2AM, and CFP, YFP, and Rhod-2 intensities were collected every 20 s.

Caged IP_3

Caged-IP_3/PM (cIP_3) was reconstituted in DMSO and stored at –20°C until use. Before injection, cIP_3 stock was diluted to 0.25 mM with water and microinjected as above. After incubation in KSOM media at 37°C for 1 hr, the injected eggs were loaded with the fluorophore, 1.25 µM Fluo4-AM, and 0.02% pluronic acid and handled as above for Fura-2 AM. The release of cIP_3 was accomplished by photolysis using 0.5–5 s pulses at 360 nm wavelengths. Ca^{2+} imaging was as above, but Fluo4 was excited at 488 nm wavelength and emitted light above 510 nm collected as above.

Western blot analysis

Cell lysates from 20 to 50 mouse eggs were prepared by adding 2× Laemmli sample buffer. Proteins were separated on 5% SDS–PAGE gels and transferred to PVDF membranes (Millipore, Bedford, MA).

After blocking with 5% fat-free milk + TBS, membranes were probed with the rabbit polyclonal antibody specific to IP_3R1 (1:1000; a generous gift from Dr. Jan Parys, Katholieke Universiteit, Leuven, Belgium; ***Parys et al., 1995***). Goat anti-rabbit antibody conjugated to horseradish peroxidase (HRP) was used as a secondary antibody (1:5000; goat anti-rabbit IgG [H+L] Cross-Adsorbed Secondary Antibody, HRP; Invitrogen, Waltham, MA). For detection of chemiluminescence, membranes were developed using ECL Prime (Sigma) and exposed for 1–3 min to maximum sensitivity film (VWR, Radnor, PA). Broad-range pre-stained SDS–PAGE molecular weight markers (Bio-Rad, Hercules, CA) were run in parallel to estimate the molecular weight of the immunoreactive bands. The same membranes were stripped at 50°C for 30 min (62.5 mM Tris, 2% SDS, and 100 mM 2-beta mercaptoethanol) and re-probed with anti-α-tubulin monoclonal antibody (1:1000).

Immunostaining and confocal microscopy

Immunostaining was performed according to our previous study (***Akizawa et al., 2021***). After incubation with or without TPEN, MII eggs were fixed with 4% (w/v) paraformaldehyde in house-made phosphate-buffered saline (PBS) for 20 min at RT and then permeabilized for 60 min with 0.2% (v/v) Triton X-100 in PBS. Next, the eggs were blocked for 45 min with a blocking buffer containing 0.2% (w/v) skim milk, 2% (v/v) fetal bovine serum, 1% (w/v) bovine serum albumin, 0.1% (v/v) TritonX-100, and 0.75% (w/v) glycine in PBS. Eggs were incubated overnight at 4°C with mouse anti-HA antibody (1:200) diluted in blocking buffer. Eggs were washed in blocking buffer 3× for 10 min, followed by incubation at RT for 30 min with a secondary antibody, Alexa Fluor 488 goat anti-mouse IgG (H+L) (1:400) diluted in blocking buffer. Fluorescence signals were visualized using a laser-scanning confocal microscope (Nikon A1 Resonant Confocal with six-color TIRF) fitted with a 63×, 1.4 NA oil-immersion objective lens.

Statistical analysis

Comparisons for statistical significance of experimental values between treatments and experiments were performed in three or more experiments performed on different batches of eggs in most studies. Given the number of eggs needed, WB studies were repeated twice. Prism-GraphPad software was used to perform the statistical comparisons that include unpaired Student's *t*-tests, Fisher's exact test, and one-way ANOVA followed by Tukey's multiple comparisons, as applicable, and the production of graphs to display the data. All data are presented as mean ± SD. Differences were considered significant at $p<0.05$.

Acknowledgements

We thank Ms. Changli He for technical support and Dr. James Chambers for support with confocal microscopy support. We thank all members of the Fissore lab for useful discussions and suggestions. We thank Jan B Parys, KU Leuven, Belgium, for initial discussions and advice.

Additional information

Funding

Funder	Grant reference number	Author
Japan Society for the Promotion of Science		Hiroki Akizawa
Eunice Kennedy Shriver National Institute of Child Health and Human Development	RO1 HD092499	Rafael A Fissore
National Institute of Food and Agriculture	2021-06893	Rafael A Fissore

The funders had no role in study design, data collection and interpretation, or the decision to submit the work for publication.

Author contributions

Hiroki Akizawa, Data curation, Formal analysis, Funding acquisition, Validation, Investigation, Visualization, Methodology, Writing - original draft, Writing - review and editing; Emily M Lopes, Data curation, Formal analysis, Investigation; Rafael A Fissore, Conceptualization, Resources, Supervision, Funding acquisition, Validation, Writing - original draft, Project administration, Writing - review and editing

Author ORCIDs

Hiroki Akizawa http://orcid.org/0000-0003-1091-5629
Rafael A Fissore http://orcid.org/0000-0001-5655-0915

Ethics

The University of Massachusetts Institutional Animal Care and Use Committee (IACUC) approved all animal experiments and protocols (#4650).

Peer review material

Reviewer #1 (Public Review): https://doi.org/10.7554/eLife.88082.3.sa1
Reviewer #2 (Public Review): https://doi.org/10.7554/eLife.88082.3.sa2
Reviewer #3 (Public Review): https://doi.org/10.7554/eLife.88082.3.sa3
Author Response https://doi.org/10.7554/eLife.88082.3.sa4

Additional files

Supplementary files

- MDAR checklist

Data availability

All data generated or analyzed during this study are included in the manuscript and supporting files. Source data files have been provided for Figures 2 and 4.

References

Abbott AL, Xu Z, Kopf GS, Ducibella T, Schultz RM. 1998. In vitro culture retards spontaneous activation of cell cycle progression and cortical granule exocytosis that normally occur in in vivo unfertilized mouse eggs. *Biology of Reproduction* **59**:1515–1521. DOI: https://doi.org/10.1095/biolreprod59.6.1515, PMID: 9828200

Ajduk A, Małagocki A, Maleszewski M. 2008. Cytoplasmic maturation of mammalian oocytes: development of a mechanism responsible for sperm-induced Ca2+ oscillations. *Reproductive Biology* **8**:3–22. DOI: https://doi.org/10.1016/s1642-431x(12)60001-1, PMID: 18432304

Akizawa H, Saito S, Kohri N, Furukawa E, Hayashi Y, Bai H, Nagano M, Yanagawa Y, Tsukahara H, Takahashi M, Kagawa S, Kawahara-Miki R, Kobayashi H, Kono T, Kawahara M. 2021. Deciphering two rounds of cell lineage segregations during bovine preimplantation development. *FASEB Journal* **35**:e21904. DOI: https://doi.org/10.1096/fj.202002762RR, PMID: 34569650

Ardestani G, Mehregan A, Fleig A, Horgen FD, Carvacho I, Fissore RA. 2020. Divalent cation influx and calcium homeostasis in germinal vesicle mouse oocytes. *Cell Calcium* **87**:102181. DOI: https://doi.org/10.1016/j.ceca.2020.102181, PMID: 32097818

Arslan P, Di Virgilio F, Beltrame M, Tsien RY, Pozzan T. 1985. Cytosolic Ca2+ homeostasis in Ehrlich and Yoshida carcinomas A new, membrane-permeant chelator of heavy metals reveals that these ascites tumor cell lines have normal cytosolic free Ca2+. *The Journal of Biological Chemistry* **260**:2719–2727. DOI: https://doi.org/10.1016/s0021-9258(18)89421-2, PMID: 3919006

Barnett BL, Kretschmar HC, Hartman FA. 1977. Structural characterization of bis(N-oxopyridine-2-thionato) zinc(II). *Inorganic Chemistry* **16**:1834–1838. DOI: https://doi.org/10.1021/ic50174a002

Bernhardt ML, Kim AM, O'Halloran TV, Woodruff TK. 2011. Zinc requirement during meiosis I-meiosis II transition in mouse oocytes is independent of the MOS-MAPK pathway. *Biology of Reproduction* **84**:526–536. DOI: https://doi.org/10.1095/biolreprod.110.086488, PMID: 21076080

Bernhardt ML, Kong BY, Kim AM, O'Halloran TV, Woodruff TK. 2012. A zinc-dependent mechanism regulates meiotic progression in mammalian oocytes. *Biology of Reproduction* **86**:114. DOI: https://doi.org/10.1095/biolreprod.111.097253, PMID: 22302686

Bernhardt ML, Padilla-Banks E, Stein P, Zhang Y, Williams CJ. 2017. Store-operated Ca 2+ entry is not required for fertilization-induced Ca 2+ signaling in mouse eggs. *Cell Calcium* **65**:63–72. DOI: https://doi.org/10.1016/j.ceca.2017.02.004

Berridge MJ. 2016. The inositol trisphosphate/calcium signaling pathway in health and disease. *Physiological Reviews* **96**:1261–1296. DOI: https://doi.org/10.1152/physrev.00006.2016, PMID: 27512009

Bhanumathy C, da Fonseca PCA, Morris EP, Joseph SK. 2012. Identification of functionally critical residues in the channel domain of inositol trisphosphate receptors. *The Journal of Biological Chemistry* **287**:43674–43684. DOI: https://doi.org/10.1074/jbc.M112.415786, PMID: 23086950

Bootman MD, Taylor CW, Berridge MJ. 1992. The thiol reagent, thimerosal, evokes Ca2+ spikes in HeLa cells by sensitizing the inositol 1,4,5-trisphosphate receptor. *The Journal of Biological Chemistry* **267**:25113–25119. DOI: https://doi.org/10.1016/s0021-9258(19)74013-7, PMID: 1334081

Brind S, Swann K, Carroll J. 2000. Inositol 1,4,5-trisphosphate receptors are downregulated in mouse oocytes in response to sperm or adenophostin A but not to increases in intracellular Ca(2+) or egg activation. *Developmental Biology* **223**:251–265. DOI: https://doi.org/10.1006/dbio.2000.9728, PMID: 10882514

Broun ER, Greist A, Tricot G, Hoffman R. 1990. Excessive zinc ingestion A reversible cause of sideroblastic anemia and bone marrow depression. *JAMA* **264**:1441–1443. DOI: https://doi.org/10.1001/jama.264.11.1441, PMID: 2094240

Carraway RE, Dobner PR. 2012. Zinc pyrithione induces ERK- and PKC-dependent necrosis distinct from TPEN-induced apoptosis in prostate cancer cells. *Biochimica et Biophysica Acta* **1823**:544–557. DOI: https://doi.org/10.1016/j.bbamcr.2011.09.013, PMID: 22027089

Carvacho I, Lee HC, Fissore RA, Clapham DE. 2013. TRPV3 channels mediate strontium-induced mouse-egg activation. *Cell Reports* **5**:1375–1386. DOI: https://doi.org/10.1016/j.celrep.2013.11.007, PMID: 24316078

Carvacho I, Ardestani G, Lee HC, McGarvey K, Fissore RA, Lykke-Hartmann K. 2016. TRPM7-like channels are functionally expressed in oocytes and modulate post-fertilization embryo development in mouse. *Scientific Reports* **6**:34236. DOI: https://doi.org/10.1038/srep34236, PMID: 27681336

Converse A, Thomas P. 2020. The zinc transporter ZIP9 (Slc39a9) regulates zinc dynamics essential to egg activation in zebrafish. *Scientific Reports* **10**:15673. DOI: https://doi.org/10.1038/s41598-020-72515-4, PMID: 32973303

Deguchi R, Shirakawa H, Oda S, Mohri T, Miyazaki S. 2000. Spatiotemporal analysis of Ca(2+) waves in relation to the sperm entry site and animal-vegetal axis during Ca(2+) oscillations in fertilized mouse eggs. *Developmental Biology* **218**:299–313. DOI: https://doi.org/10.1006/dbio.1999.9573, PMID: 10656771

des Georges A, Clarke OB, Zalk R, Yuan Q, Condon KJ, Grassucci RA, Hendrickson WA, Marks AR, Frank J. 2016. Structural basis for gating and activation of RyR1. *Cell* **167**:145–157. DOI: https://doi.org/10.1016/j.cell.2016.08.075, PMID: 27662087

Ducibella T, Huneau D, Angelichio E, Xu Z, Schultz RM, Kopf GS, Fissore R, Madoux S, Ozil JP. 2002. Egg-to-embryo transition is driven by differential responses to Ca(2+) oscillation number. *Developmental Biology* **250**:280–291. DOI: https://doi.org/10.1006/dbio.2002.0788, PMID: 12376103

Dupont G, McGuinness OM, Johnson MH, Berridge MJ, Borgese F. 1996. Phospholipase C in mouse oocytes: characterization of beta and gamma isoforms and their possible involvement in sperm-induced Ca2+ spiking. *The Biochemical Journal* **316 (Pt 2)**:583–591. DOI: https://doi.org/10.1042/bj3160583, PMID: 8687404

Eppig JJ. 1996. Coordination of nuclear and cytoplasmic oocyte maturation in eutherian mammals. *Reproduction, Fertility, and Development* **8**:485–489. DOI: https://doi.org/10.1071/rd9960485, PMID: 8870074

Evellin S, Nolte J, Tysack K, vom Dorp F, Thiel M, Weernink PAO, Jakobs KH, Webb EJ, Lomasney JW, Schmidt M. 2002. Stimulation of phospholipase C-epsilon by the M3 muscarinic acetylcholine receptor mediated by cyclic AMP and the GTPase Rap2B. *The Journal of Biological Chemistry* **277**:16805–16813. DOI: https://doi.org/10.1074/jbc.M112024200, PMID: 11877431

Fan G, Baker ML, Wang Z, Baker MR, Sinyagovskiy PA, Chiu W, Ludtke SJ, Serysheva II. 2015. Gating machinery of InsP3R channels revealed by electron cryomicroscopy. *Nature* **527**:336–341. DOI: https://doi.org/10.1038/nature15249, PMID: 26458101

Fan G, Baker MR, Terry LE, Arige V, Chen M, Seryshev AB, Baker ML, Ludtke SJ, Yule DI, Serysheva II. 2022. Conformational motions and ligand-binding underlying gating and regulation in IP_3R channel. *Nature Communications* **13**:6942. DOI: https://doi.org/10.1038/s41467-022-34574-1, PMID: 36376291

Fissore RA, Longo FJ, Anderson E, Parys JB, Ducibella T. 1999. Differential distribution of inositol trisphosphate receptor isoforms in mouse oocytes. *Biology of Reproduction* **60**:49–57. DOI: https://doi.org/10.1095/biolreprod60.1.49, PMID: 9858485

Fujiwara T, Nakada K, Shirakawa H, Miyazaki S. 1993. Development of inositol trisphosphate-induced calcium release mechanism during maturation of hamster oocytes. *Developmental Biology* **156**:69–79. DOI: https://doi.org/10.1006/dbio.1993.1059, PMID: 8383620

Gee KR, Zhou ZL, Qian WJ, Kennedy R. 2002. Detection and imaging of zinc secretion from pancreatic beta-cells using a new fluorescent zinc indicator. *Journal of the American Chemical Society* **124**:776–778. DOI: https://doi.org/10.1021/ja011774y, PMID: 11817952

Hajnóczky G, Thomas AP. 1997. Minimal requirements for calcium oscillations driven by the IP3 receptor. *The EMBO Journal* **16**:3533–3543. DOI: https://doi.org/10.1093/emboj/16.12.3533, PMID: 9218795

Hamada K, Terauchi A, Mikoshiba K. 2003. Three-dimensional rearrangements within inositol 1,4,5-trisphosphate receptor by calcium. *The Journal of Biological Chemistry* **278**:52881–52889. DOI: https://doi.org/10.1074/jbc.M309743200, PMID: 14593123

Hara T, Yoshigai E, Ohashi T, Fukada T. 2022. Zinc transporters as potential therapeutic targets: An updated review. *Journal of Pharmacological Sciences* **148**:221–228. DOI: https://doi.org/10.1016/j.jphs.2021.11.007, PMID: 35063137

Heim A, Tischer T, Mayer TU. 2018. Calcineurin promotes APC/C activation at meiotic exit by acting on both XErp1 and Cdc20. *EMBO Reports* **19**:1–10. DOI: https://doi.org/10.15252/embr.201846433, PMID: 30373936

Higo T, Hattori M, Nakamura T, Natsume T, Michikawa T, Mikoshiba K. 2005. Subtype-specific and ER lumenal environment-dependent regulation of inositol 1,4,5-trisphosphate receptor type 1 by ERp44. *Cell* **120**:85–98. DOI: https://doi.org/10.1016/j.cell.2004.11.048, PMID: 15652484

Iino M. 1990. Biphasic Ca2+ dependence of inositol 1,4,5-trisphosphate-induced Ca release in smooth muscle cells of the guinea pig taenia caeci. *The Journal of General Physiology* **95**:1103–1122. DOI: https://doi.org/10.1085/jgp.95.6.1103, PMID: 2373998

Jean T, Klee CB. 1986. Calcium modulation of inositol 1,4,5-trisphosphate-induced calcium release from neuroblastoma x glioma hybrid (NG108-15) microsomes. *The Journal of Biological Chemistry* **261**:16414–16420. DOI: https://doi.org/10.1016/s0021-9258(18)66582-2, PMID: 3491073

Jellerette T, He CL, Wu H, Parys JB, Fissore RA. 2000. Down-regulation of the inositol 1,4,5-trisphosphate receptor in mouse eggs following fertilization or parthenogenetic activation. *Developmental Biology* **223**:238–250. DOI: https://doi.org/10.1006/dbio.2000.9675, PMID: 10882513

Jellerette Teru, Kurokawa M, Lee B, Malcuit C, Yoon S-Y, Smyth J, Vermassen E, De Smedt H, Parys JB, Fissore RA. 2004. Cell cycle-coupled [Ca(2+)](i) oscillations in mouse zygotes and function of the inositol 1,4,5-trisphosphate receptor-1. *Developmental Biology* **274**:94–109. DOI: https://doi.org/10.1016/j.ydbio.2004.06.020, PMID: 15355791

Joseph SK, Young MP, Alzayady K, Yule DI, Ali M, Booth DM, Hajnóczky G. 2018. Redox regulation of type-I inositol trisphosphate receptors in intact mammalian cells. *The Journal of Biological Chemistry* **293**:17464–17476. DOI: https://doi.org/10.1074/jbc.RA118.005624, PMID: 30228182

Kang D, Park JY, Han J, Bae IH, Yoon SY, Kang SS, Choi WS, Hong SG. 2003. Acetylcholine induces Ca 2+ oscillations via m3/m4 muscarinic receptors in the mouse oocyte. *Pflugers Archiv European Journal of Physiology* **447**:321–327. DOI: https://doi.org/10.1007/s00424-003-1184-y

Kaur K, Gupta R, Saraf SA, Saraf SK. 2014. Zinc: the metal of life. *Comprehensive Reviews in Food Science and Food Safety* **13**:358–376. DOI: https://doi.org/10.1111/1541-4337.12067, PMID: 33412710

Kim AM, Vogt S, O'Halloran TV, Woodruff TK. 2010. Zinc availability regulates exit from meiosis in maturing mammalian oocytes. *Nature Chemical Biology* **6**:674–681. DOI: https://doi.org/10.1038/nchembio.419, PMID: 20693991

Kim AM, Bernhardt ML, Kong BY, Ahn RW, Vogt S, Woodruff TK, O'Halloran TV. 2011. Zinc sparks are triggered by fertilization and facilitate cell cycle resumption in mammalian eggs. *ACS Chemical Biology* **6**:716–723. DOI: https://doi.org/10.1021/cb200084y, PMID: 21526836

Kurokawa M, Fissore RA. 2003. ICSI-generated mouse zygotes exhibit altered calcium oscillations, inositol 1,4,5-trisphosphate receptor-1 down-regulation, and embryo development. *Molecular Human Reproduction* **9**:523–533. DOI: https://doi.org/10.1093/molehr/gag072, PMID: 12900511

Lawrence Y, Ozil JP, Swann K. 1998. The effects of a Ca2+ chelator and heavy-metal-ion chelators upon Ca2+ oscillations and activation at fertilization in mouse eggs suggest a role for repetitive Ca2+ increases. *The Biochemical Journal* **335 (Pt 2)**:335–342. DOI: https://doi.org/10.1042/bj3350335, PMID: 9761732

Lee B, Vermassen E, Yoon SY, Vanderheyden V, Ito J, Alfandari D, De Smedt H, Parys JB, Fissore RA. 2006. Phosphorylation of IP3R1 and the regulation of [Ca2+]i responses at fertilization: a role for the MAP kinase pathway. *Development* **133**:4355–4365. DOI: https://doi.org/10.1242/dev.02624, PMID: 17038520

Lemos FO, Bultynck G, Parys JB. 2021. A comprehensive overview of the complex world of the endo- and sarcoplasmic reticulum Ca^{2+}-leak channels. *Biochimica et Biophysica Acta. Molecular Cell Research* **1868**:119020. DOI: https://doi.org/10.1016/j.bbamcr.2021.119020, PMID: 33798602

Liu M. 2011. The biology and dynamics of mammalian cortical granules. *Reproductive Biology and Endocrinology* **9**:149. DOI: https://doi.org/10.1186/1477-7827-9-149, PMID: 22088197

Lo MN, Damon LJ, Wei Tay J, Jia S, Palmer AE. 2020. Single cell analysis reveals multiple requirements for zinc in the mammalian cell cycle. *eLife* **9**:e51107. DOI: https://doi.org/10.7554/eLife.51107, PMID: 32014109

Lorca T, Cruzalegui FH, Fesquet D, Cavadore JC, Méry J, Means A, Dorée M. 1993. Calmodulin-dependent protein kinase II mediates inactivation of MPF and CSF upon fertilization of *Xenopus* eggs. *Nature* **366**:270–273. DOI: https://doi.org/10.1038/366270a0, PMID: 8232587

Maret W, Li Y. 2009. Coordination dynamics of zinc in proteins. *Chemical Reviews* **109**:4682–4707. DOI: https://doi.org/10.1021/cr800556u, PMID: 19728700

Matsu-ura T, Shirakawa H, Suzuki KGN, Miyamoto A, Sugiura K, Michikawa T, Kusumi A, Mikoshiba K. 2019. Dual-FRET imaging of IP3 and Ca2+ revealed Ca2+-induced IP3 production maintains long lasting Ca2+ oscillations in fertilized mouse eggs. *Scientific Reports* **9**:1–11. DOI: https://doi.org/10.1038/s41598-019-40931-w

Mendivil-Perez M, Velez-Pardo C, Jimenez-Del-Rio M. 2012. TPEN induces apoptosis independently of zinc chelator activity in a model of acute lymphoblastic leukemia and ex vivo acute leukemia cells through oxidative stress and mitochondria caspase-3- and AIF-dependent pathways. *Oxidative Medicine and Cellular Longevity* **2012**:313275. DOI: https://doi.org/10.1155/2012/313275, PMID: 23320127

Mendoza AD, Sue A, Antipova O, Vogt S, Woodruff TK, Wignall SM, O'Halloran TV. 2022. Dynamic zinc fluxes regulate meiotic progression in *Caenorhabditis elegans*†. *Biology of Reproduction* **107**:406–418. DOI: https://doi.org/10.1093/biolre/ioac064, PMID: 35466369

Miao YL, Stein P, Jefferson WN, Padilla-Banks E, Williams CJ. 2012. Calcium influx-mediated signaling is required for complete mouse egg activation. *PNAS* **109**:4169–4174. DOI: https://doi.org/10.1073/pnas.1112333109, PMID: 22371584

Miyazaki SI, Hashimoto N, Yoshimoto Y, Kishimoto T, Igusa Y, Hiramoto Y. 1986. Temporal and spatial dynamics of the periodic increase in intracellular free calcium at fertilization of golden hamster eggs. *Developmental Biology* **118**:259–267. DOI: https://doi.org/10.1016/0012-1606(86)90093-X

Miyazaki S. 1988. Inositol 1,4,5-trisphosphate-induced calcium release and guanine nucleotide-binding protein-mediated periodic calcium rises in golden hamster eggs. *The Journal of Cell Biology* **106**:345–353. DOI: https://doi.org/10.1083/jcb.106.2.345, PMID: 3123497

Miyazaki SI, Yuzaki M, Nakada K, Shirakawa H, Nakanishi S, Nakade S, Mikoshiba K. 1992. Block of Ca2+ wave and Ca2+ oscillation by antibody to the inositol 1,4,5-trisphosphate receptor in fertilized hamster eggs. *Science* **257**:251–255. DOI: https://doi.org/10.1126/science.1321497, PMID: 1321497

Miyazaki S, Ito M. 2006. Calcium signals for egg activation in mammals. *Journal of Pharmacological Sciences* **100**:545–552. DOI: https://doi.org/10.1254/jphs.cpj06003x, PMID: 16799264

Nomikos M, Elgmati K, Theodoridou M, Calver BL, Nounesis G, Swann K, Lai FA. 2011. Phospholipase C ζ binding to PtdIns(4,5)P2 requires the XY-linker region. *Journal of Cell Science* **124**:2582–2590. DOI: https://doi.org/10.1242/jcs.083485, PMID: 21730019

Nomikos M, Sanders JR, Parthimos D, Buntwal L, Calver BL, Stamatiadis P, Smith A, Clue M, Sideratou Z, Swann K, Lai FA. 2015. Essential role of the EF-hand domain in targeting sperm phospholipase C ζ to membrane phosphatidylinositol 4,5-Bisphosphate (PIP2). *Journal of Biological Chemistry* **290**:29519–29530. DOI: https://doi.org/10.1074/jbc.M115.658443

Pace NJ, Weerapana E. 2014. A competitive chemical-proteomic platform to identify zinc-binding cysteines. *ACS Chemical Biology* **9**:258–265. DOI: https://doi.org/10.1021/cb400622q, PMID: 24111988

Paknejad N, Hite RK. 2018. Structural basis for the regulation of inositol trisphosphate receptors by Ca2+ and IP3. *Nature Structural & Molecular Biology* **25**:660–668. DOI: https://doi.org/10.1038/s41594-018-0089-6

Palmer AE, Jin C, Reed JC, Tsien RY. 2004. Bcl-2-mediated alterations in endoplasmic reticulum Ca2+ analyzed with an improved genetically encoded fluorescent sensor. *PNAS* **101**:17404–17409. DOI: https://doi.org/10.1073/pnas.0408030101, PMID: 15585581

Parrington J, Brind S, De Smedt H, Gangeswaran R, Lai FA, Wojcikiewicz R, Carroll J. 1998. Expression of inositol 1,4,5-trisphosphate receptors in mouse oocytes and early embryos: the type I isoform is upregulated in oocytes and downregulated after fertilization. *Developmental Biology* **203**:451–461. DOI: https://doi.org/10.1006/dbio.1998.9071, PMID: 9808793

Parys JB, de Smedt H, Missiaen L, Bootman MD, Sienaert I, Casteels R. 1995. Rat basophilic leukemia cells as model system for inositol 1,4,5-trisphosphate receptor IV, a receptor of the type II family: functional comparison and immunological detection. *Cell Calcium* **17**:239–249. DOI: https://doi.org/10.1016/0143-4160(95)90070-5, PMID: 7664312

Perreault SD, Barbee RR, Slott VL. 1988. Importance of glutathione in the acquisition and maintenance of sperm nuclear decondensing activity in maturing hamster oocytes. *Developmental Biology* **125**:181–186. DOI: https://doi.org/10.1016/0012-1606(88)90070-x, PMID: 3334716

Qin Y, Dittmer PJ, Park JG, Jansen KB, Palmer AE. 2011. Measuring steady-state and dynamic endoplasmic reticulum and Golgi Zn2+ with genetically encoded sensors. *PNAS* **108**:7351–7356. DOI: https://doi.org/10.1073/pnas.1015686108, PMID: 21502528

Que EL, Bleher R, Duncan FE, Kong BY, Gleber SC, Vogt S, Chen S, Garwin SA, Bayer AR, Dravid VP, Woodruff TK, O'Halloran TV. 2015. Quantitative mapping of zinc fluxes in the mammalian egg reveals the origin of fertilization-induced zinc sparks. *Nature Chemistry* **7**:130–139. DOI: https://doi.org/10.1038/nchem.2133, PMID: 25615666

Que EL, Duncan FE, Lee HC, Hornick JE, Vogt S, Fissore RA, O'Halloran TV, Woodruff TK. 2019. Bovine eggs release zinc in response to parthenogenetic and sperm-induced egg activation. *Theriogenology* **127**:41–48. DOI: https://doi.org/10.1016/j.theriogenology.2018.12.031, PMID: 30639695

Richardson A, Taylor CW. 1993. Effects of Ca2+ chelators on purified inositol 1,4,5-trisphosphate (InsP3) receptors and InsP3-stimulated Ca2+ mobilization. *The Journal of Biological Chemistry* **268**:11528–11533. DOI: https://doi.org/10.1016/s0021-9258(19)50232-0, PMID: 8389355

Ridgway EB, Gilkey JC, Jaffe LF. 1977. Free calcium increases explosively in activating medaka eggs. *PNAS* **74**:623–627. DOI: https://doi.org/10.1073/pnas.74.2.623, PMID: 322135

Robinson MA. 1964. Complexes of 1-hydroxy 2-pyridinethione. *Journal of Inorganic and Nuclear Chemistry* **26**:1277–1281. DOI: https://doi.org/10.1016/0022-1902(64)80210-4

Sanders JR, Ashley B, Moon A, Woolley TE, Swann K. 2018. PLC ζ Induced Ca2+ oscillations in mouse eggs involve a positive feedback cycle of Ca2+ induced InsP3 formation from cytoplasmic PIP2. *Frontiers in Cell and Developmental Biology* **6**:1–14. DOI: https://doi.org/10.3389/fcell.2018.00036

Saunders CM, Larman MG, Parrington J, Cox LJ, Royse J, Blayney LM, Swann K, Lai FA. 2002. PLC zeta: a sperm-specific trigger of Ca(2+) oscillations in eggs and embryo development. *Development* **129**:3533–3544. DOI: https://doi.org/10.1242/dev.129.15.3533, PMID: 12117804

Schultz RM, Kopf GS. 1995. Molecular basis of mammalian egg activation. *Current Topics in Developmental Biology* **30**:21–62. DOI: https://doi.org/10.1016/s0070-2153(08)60563-3, PMID: 7555047

Seeler JF, Sharma A, Zaluzec NJ, Bleher R, Lai B, Schultz EG, Hoffman BM, LaBonne C, Woodruff TK, O'Halloran TV. 2021. Metal ion fluxes controlling amphibian fertilization. *Nature Chemistry* **13**:683–691. DOI: https://doi.org/10.1038/s41557-021-00705-2, PMID: 34155376

Shoji S, Yoshida N, Amanai M, Ohgishi M, Fukui T, Fujimoto S, Nakano Y, Kajikawa E, Perry ACF. 2006. Mammalian Emi2 mediates cytostatic arrest and transduces the signal for meiotic exit via Cdc20. *The EMBO Journal* **25**:834–845. DOI: https://doi.org/10.1038/sj.emboj.7600953, PMID: 16456547

Shoji S, Muto Y, Ikeda M, He F, Tsuda K, Ohsawa N, Akasaka R, Terada T, Wakiyama M, Shirouzu M, Yokoyama S. 2014. The zinc-binding region (ZBR) fragment of Emi2 can inhibit APC/C by targeting its association with the coactivator Cdc20 and UBE2C-mediated ubiquitylation. *FEBS Open Bio* **4**:689–703. DOI: https://doi.org/10.1016/j.fob.2014.06.010, PMID: 25161877

Sienaert I, Missiaen L, De Smedt H, Parys JB, Sipma H, Casteels R. 1997. Molecular and functional evidence for multiple Ca2+-binding domains in the type 1 inositol 1,4,5-trisphosphate receptor. *The Journal of Biological Chemistry* **272**:25899–25906. DOI: https://doi.org/10.1074/jbc.272.41.25899, PMID: 9325322

Sikora J, Ouagazzal AM. 2021. Synaptic Zinc: an emerging player in parkinson's disease. *International Journal of Molecular Sciences* **22**:1–16. DOI: https://doi.org/10.3390/ijms22094724, PMID: 33946908

Sipma H, De Smet P, Sienaert I, Vanlingen S, Missiaen L, Parys JB, De Smedt H. 1999. Modulation of inositol 1,4,5-trisphosphate binding to the recombinant ligand-binding site of the type-1 inositol 1,4, 5-trisphosphate receptor by Ca2+ and calmodulin. *The Journal of Biological Chemistry* **274**:12157–12162. DOI: https://doi.org/10.1074/jbc.274.17.12157, PMID: 10207043

Snitsarev VA, McNulty TJ, Taylor CW. 1996. Endogenous heavy metal ions perturb fura-2 measurements of basal and hormone-evoked Ca2+ signals. *Biophysical Journal* **71**:1048–1056. DOI: https://doi.org/10.1016/S0006-3495(96)79305-0, PMID: 8842241

Stein P, Savy V, Williams AM, Williams CJ. 2020. Modulators of calcium signalling at fertilization. *Open Biology* **10**:200118. DOI: https://doi.org/10.1098/rsob.200118, PMID: 32673518

Stricker SA. 1999. Comparative biology of calcium signaling during fertilization and egg activation in animals. *Developmental Biology* **211**:157–176. DOI: https://doi.org/10.1006/dbio.1999.9340, PMID: 10395780

Suzuki T, Suzuki E, Yoshida N, Kubo A, Li H, Okuda E, Amanai M, Perry ACF. 2010a. Mouse Emi2 as a distinctive regulatory hub in second meiotic metaphase. *Development* **137**:3281–3291. DOI: https://doi.org/10.1242/dev.052480, PMID: 20724447

Suzuki T, Yoshida N, Suzuki E, Okuda E, Perry ACF. 2010b. Full-term mouse development by abolishing Zn2+-dependent metaphase II arrest without Ca2+ release. *Development* **137**:2659–2669. DOI: https://doi.org/10.1242/dev.049791, PMID: 20591924

Swann K, Parrington J. 1999. Mechanism of Ca2+ release at fertilization in mammals. *The Journal of Experimental Zoology* **285**:267–275. DOI: https://doi.org/10.1002/(sici)1097-010x(19991015)285:3<267::aid-jez10>3.0.co;2-p, PMID: 10497326

Taylor CW, Tovey SC. 2010. IP(3) receptors: toward understanding their activation. *Cold Spring Harbor Perspectives in Biology* **2**:a004010. DOI: https://doi.org/10.1101/cshperspect.a004010, PMID: 20980441

Thastrup O, Cullen PJ, Drøbak BK, Hanley MR, Dawson AP. 1990. Thapsigargin, a tumor promoter, discharges intracellular Ca2+ stores by specific inhibition of the endoplasmic reticulum Ca2(+)-ATPase. *PNAS* **87**:2466–2470. DOI: https://doi.org/10.1073/pnas.87.7.2466, PMID: 2138778

Toeplitz BK, Cohen AI, Funke PT, Parker WL, Gougoutas JZ. 1979. Structure of ionomycin - A novel diacidic polyether antibiotic having high affinity for calcium ions. *Journal of the American Chemical Society* **101**:3344–3353. DOI: https://doi.org/10.1021/ja00506a035

Tokuhiro K, Dean J. 2018. Glycan-Independent gamete recognition triggers egg zinc sparks and zp2 cleavage to prevent polyspermy. *Developmental Cell* **46**:627–640.. DOI: https://doi.org/10.1016/j.devcel.2018.07.020, PMID: 30122633

Uchida K, Miyauchi H, Furuichi T, Michikawa T, Mikoshiba K. 2003. Critical regions for activation gating of the inositol 1,4,5-trisphosphate receptor. *The Journal of Biological Chemistry* **278**:16551–16560. DOI: https://doi.org/10.1074/jbc.M300646200, PMID: 12621039

Wakai T, Vanderheyden V, Yoon SY, Cheon B, Zhang N, Parys JB, Fissore RA. 2012. Regulation of inositol 1,4,5-trisphosphate receptor function during mouse oocyte maturation. *Journal of Cellular Physiology* **227**:705–717. DOI: https://doi.org/10.1002/jcp.22778, PMID: 21465476

Wakai T, Fissore RA. 2013. Ca(2+) homeostasis and regulation of ER Ca(2+) in mammalian oocytes/eggs. *Cell Calcium* **53**:63–67. DOI: https://doi.org/10.1016/j.ceca.2012.11.010, PMID: 23260016

Wakai T, Zhang N, Vangheluwe P, Fissore RA. 2013. Regulation of endoplasmic reticulum Ca(2+) oscillations in mammalian eggs. *Journal of Cell Science* **126**:5714–5724. DOI: https://doi.org/10.1242/jcs.136549, PMID: 24101727

Wakai T, Harada Y, Miyado K, Kono T. 2014. Mitochondrial dynamics controlled by mitofusins define organelle positioning and movement during mouse oocyte maturation. *Molecular Human Reproduction* **20**:1090–1100. DOI: https://doi.org/10.1093/molehr/gau064, PMID: 25113836

Wakai T, Fissore RA. 2019. Constitutive IP3R1-mediated Ca2+ release reduces Ca2+ store content and stimulates mitochondrial metabolism in mouse GV oocytes. *Journal of Cell Science* **132**:441. DOI: https://doi.org/10.1242/jcs.225441

Wakai T, Mehregan A, Fissore RA. 2019. Ca2+ signaling and homeostasis in mammalian oocytes and eggs. *Cold Spring Harbor Perspectives in Biology* **11**:a035162. DOI: https://doi.org/10.1101/cshperspect.a035162

Walker JW, Somlyo AV, Goldman YE, Somlyo AP, Trentham DR. 1987. Kinetics of smooth and skeletal muscle activation by laser pulse photolysis of caged inositol 1,4,5-trisphosphate. *Nature* **327**:249–252. DOI: https://doi.org/10.1038/327249a0, PMID: 3494954

Watanabe S, Amagai Y, Sannino S, Tempio T, Anelli T, Harayama M, Masui S, Sorrentino I, Yamada M, Sitia R, Inaba K. 2019. Zinc regulates ERp44-dependent protein quality control in the early secretory pathway. *Nature Communications* **10**:603. DOI: https://doi.org/10.1038/s41467-019-08429-1, PMID: 30723194

Webster JM, Tiwari S, Weissman AM, Wojcikiewicz RJH. 2003. Inositol 1,4,5-trisphosphate receptor ubiquitination is mediated by mammalian Ubc7, a component of the endoplasmic reticulum-associated

degradation pathway, and is inhibited by chelation of intracellular Zn2+. *The Journal of Biological Chemistry* **278**:38238–38246. DOI: https://doi.org/10.1074/jbc.M305600200, PMID: 12869571

Woodier J, Rainbow RD, Stewart AJ, Pitt SJ. 2015. Intracellular zinc modulates cardiac ryanodine receptor-mediated calcium release. *The Journal of Biological Chemistry* **290**:17599–17610. DOI: https://doi.org/10.1074/jbc.M115.661280, PMID: 26041778

Wozniak KL, Bainbridge RE, Summerville DW, Tembo M, Phelps WA, Sauer ML, Wisner BW, Czekalski ME, Pasumarthy S, Hanson ML, Linderman MB, Luu CH, Boehm ME, Sanders SM, Buckley KM, Bain DJ, Nicotra ML, Lee MT, Carlson AE. 2020. Zinc protection of fertilized eggs is an ancient feature of sexual reproduction in animals. *PLOS Biology* **18**:e3000811. DOI: https://doi.org/10.1371/journal.pbio.3000811, PMID: 32735558

Wu H, Smyth J, Luzzi V, Fukami K, Takenawa T, Black SL, Allbritton NL, Fissore RA. 2001. Sperm factor induces intracellular free calcium oscillations by stimulating the phosphoinositide pathway. *Biology of Reproduction* **64**:1338–1349. DOI: https://doi.org/10.1095/biolreprod64.5.1338, PMID: 11319137

Wu L, Sweet T, Clapham DE. 2010. Current progress in the mammalian TRP ion channel family. *Pharmocol Rev* **62**:381–404. DOI: https://doi.org/10.1124/pr.110.002725.Abbreviations

Xu Z, Williams CJ, Kopf GS, Schultz RM. 2003. Maturation-associated increase in IP3 receptor type 1: role in conferring increased IP3 sensitivity and Ca2+ oscillatory behavior in mouse eggs. *Developmental Biology* **254**:163–171. DOI: https://doi.org/10.1016/s0012-1606(02)00049-0, PMID: 12591238

Yamasaki S, Sakata-Sogawa K, Hasegawa A, Suzuki T, Kabu K, Sato E, Kurosaki T, Yamashita S, Tokunaga M, Nishida K, Hirano T. 2007. Zinc is a novel intracellular second messenger. *The Journal of Cell Biology* **177**:637–645. DOI: https://doi.org/10.1083/jcb.200702081, PMID: 17502426

Zhang N, Duncan FE, Que EL, O'Halloran TV, Woodruff TK. 2016. The fertilization-induced zinc spark is a novel biomarker of mouse embryo quality and early development. *Scientific Reports* **6**:22772. DOI: https://doi.org/10.1038/srep22772, PMID: 26987302